Metformin Alleviates Arthrofibrosis in Rat via Fibroblast Metabolic Reprogramming and Lactate-Mediated Macrophage Polarization

Zhenglin Zhu, MD, PhD [1, 2] †, Shengqiang Gao, MD [1, 2] †, Hui Zhu, MD, PhD[3], Yi Chen, MD[4], Dandong Wu, MD, PhD[5], Zhiyu Chen, MD, PhD[1,2], Jing Zou, MD[1, 2], Xiangdong Wu, MD, PhD[6], Ning Hu, MD, PhD[1,2], Wei Huang, MD[1,2] *, Hong Chen, MD, PhD[1, 2]*

[1]Department of Orthopedics, The First Affiliated Hospital of Chongqing Medical University, Chongqing, China

[2]Orthopedic Laboratory of Chongqing Medical University, Chongqing, China

[3]Department of Ultrasound, The First Affiliated Hospital of Chongqing Medical University, Chongqing, China

[4]Department of Rehabilitation, The Second Affiliated Hospital of Chongqing Medical University, Chongqing, China

[5]Department of Rehabilitation, The First Affiliated Hospital of Chongqing Medical University, Chongqing, China

[6]Department of Orthopaedic Surgery, Peking University Fourth School of Clinical, Medicine/Beijing Jishuitan Hospital, Beijing ,China

†Equal contributions

* Correspondence:
Wei Huang, email: [huangwei68@263.net]
Hong Chen, email: [chhong113@126.com]

Abstract

Background: Emerging studies have suggested an essential role of fibroblast metabolic reprogramming in the pathogenesis of arthrofibrosis. The metabolic modulator metformin appears to be a good candidate for fibrotic disorder treatment. We sought to determine the beneficial effect of metformin on arthrofibrosis and the underlying mechanism of action of this drug.

Methods: Shoulder capsule samples were collected from patients with/without frozen shoulder to perform gene and protein expression analysis. Arthrofibrotic animal model was established to examine the anti-fibrotic effect of metformin. In vitro cell culture experiments were conducted to determine the mechanism by which metformin inhibits fibroblast activation.

Results: Clinical sample analysis demonstrated that glycolysis was upregulated in human fibrotic joint capsules. In an arthrofibrotic animal model, metformin improved the joint range of motion, reduced capsular fibrosis and thickening, mitigated inflammatory reactions, and downregulated both fibrotic and glycolytic markers. The results of gene and protein expression analysis showed that metformin effectively inhibited TGF-β induced fibroblast activation. The metabolomics study confirmed a metformin-induced metabolic shift from oxidative phosphorylation (OXPHOS) to aerobic glycolysis in fibroblasts. Importantly, the inhibitory effect of metformin on fibroblast activation was mediated by metabolic reprogramming of fibroblasts. Interestingly, fibroblast-derived lactate induced M2-like macrophage polarization and diminished the inflammatory reaction.

Conclusions: Metformin is a potential treatment alternative for arthrofibrosis, and antifibrotic effect of the drug involves metabolic reprogramming toward aerobic glycolysis in fibroblasts and lactate-induced M2-like macrophage polarization.

Funding This work was supported by Chongqing Natural Science Foundation (Grant No. cstc2019jcyj-msxmX0831), the Science and Technology Research Program of Chongqing Municipal Education Commission (Grant No. KJQN202000430) and Chongqing Medical Scientific Research Project (Grant No. 2021MSXM032). This project was also supported by Innovation Project from Chongqing Municipal Education Commission (#CYB21169) to Z.Z.

Keywords Arthrofibrosis; Metformin; Fibroblast; Metabolic reprogramming; Macrophage

Abbreviations

AMPK: AMP-activated protein kinase, ANOVA: Analysis of variance, α-SMA: α-Smooth muscle actin, Arg-1: Arginase-1, CCK-8: Cell Counting Kit-8, DAPI: 4',6-diamidino-2-phenylindole, ECM: Extracellular matrix, EDTA: Ethylenediaminetetraacetic acid, FBS: Fetal bovine serum, ^{18}FDG-PET: ^{18}F-fluoro-deoxyglucose positron-emission tomography, FN1: Fibronectin, GLUT1: Glucose transporter 1, HE: Hematoxylin-eosin, HK2: Hexokinase-2, IFN-γ: Interferon-γ, IHC: Immunohistochemistry, IL: Interleukin, iNOS: Inducible nitric oxide synthase, LC-MS: Liquid Chromatograph-Mass Spectrometer, LDHA: Lactate dehydrogenase, MΦ: Macrophage, NSAIDs: Non-Steroidal Anti-Inflammatory Drugs, OARSI: Osteoarthritis Research Society International, OD: Optical density, OXPHOS: Oxidative phosphorylation, PBS: Phosphate buffered saline, PFKFB3: 6-phosphofructo-2-kinase/fructose-2,6-bisphosphatase 3, PFKP: Phosphofructokinase, PLGA: Poly (lactic-co-glycolic acid), PKM: Pyruvate kinase M, qRT-PCR: Reverse transcription-quantitative polymerase chain reaction, ROM: Range of motion, SEM: Standard error of mean, TCA: Tricarboxylic acid, TGF-β: Transforming growth factor-β, TNF-α: Tumor necrosis factor-α

Introduction

Arthrofibrosis is a common disabling fibrotic joint disorder, manifesting as a painful and long-lasting restriction of ROM (Blessing et al., 2019). Arthrofibrosis can occur in most joints, but more frequently affects the shoulder, elbow, and knee. Because of the significant importance of joint function in daily activity, arthrofibrosis is highly frustrating and debilitating. For example, a minor loss of knee extension of 5° creates difficulties in walking, and a 50% loss in elbow motion leads to 80% loss of function (Usher et al., 2019). Unfortunately, satisfactory treatment options for arthrofibrosis are still lacking. Conservative treatments including NSAIDs, intra-articular corticosteroid injections, and physical therapy are limited in their effectiveness. Surgical interventions may rapidly improve joint ROM in a fast fashion but are associated with specific complications. In addition, surgical trauma can trigger inflammatory reactions, giving rise to even more distinct fibrotic changes (Arsoy et al., 2018; Baranowski et al., 2019; Itoi et al., 2016). Thus, safe and effective alternative therapeutics are needed to treat this debilitating joint disorder.

The pathogenesis of arthrofibrosis has not been fully elucidated. However, the studies of other fibrotic diseases provide important insights and clues. After exposure to various stimuli, quiescent fibroblasts differentiate into highly proliferative myofibroblasts, which produce excessive fibers of α-SMA and collagen type 1, leading to ECM deposition and tissue contraction (N. C. Henderson, Rieder, & Wynn, 2020; Mattoo & Pillai, 2021; Phan et al., 2021; Rockey, Bell, & Hill, 2015; Tsuchida & Friedman, 2017). Therefore, profibrogenic transformation of fibroblasts is central to the development of fibrosis.

Emerging studies have suggested an essential role of fibroblast metabolic reprogramming in myofibroblast transformation (Bernard et al., 2015; S. J. Cho et al., 2020; Gopu, Fan, Shetty, Nagaraja, & Shetty, 2020; Hamanaka & Mutlu, 2021; J. Henderson, Duffy, Stratton, Ford, & O'Reilly, 2020; Schruf et al., 2019; Smith-Cortinez et al., 2020). ^{18}FDG-PET studies showed that glucose uptake is increased in the fibrotic capsules of frozen shoulder patients and is highly correlated with disease severity (Kim du, Sung, Ga, & Choi, 2014; Won et al., 2017). Multiple reports have revealed that TGF-β, a well-established profibrotic cytokine, increases oxygen consumption and cellular levels of TCA cycle metabolites in fibroblasts, suggesting that OXPHOS is crucial to support the energetic demand of myofibroblasts (Bernard et al., 2015; O'Leary et al., 2020; Schworer et al., 2020; Selvarajah et al., 2019; Xie et al., 2015). Thus, fibroblastic glucose metabolism may be a promising therapeutic target for arthrofibrosis.

Metabolic modulator metformin has long been used as the first-line treatment for patients with type 2 diabetes mellitus because of high efficacy and safety profile of the drug. Several animal studies demonstrated that metformin can treat and prevent fibrosis in preclinical models of kidney, lung, heart, liver, and ovary (Feng, Wang, Zhang, & Xiao, 2017; Han et al., 2021; Kheirollahi et al., 2019; Li et al., 2021; McCloskey et al., 2020; Mummidi et al., 2016; Rangarajan et al., 2018; Sato et al., 2016; Tang, Xu, Ye, & Wang, 2021). Interestingly, the results of a recent metabolomic analysis showed that metformin treatment led to the suppression of the TCA cycle and elevation of lactate production in fibroblasts, implicating a metabolic shift from OXPHOS to aerobic glycolysis (Yan et al., 2019). These data suggest that metformin may be a good candidate for arthrofibrosis therapy and that metabolic rewiring of fibroblasts plays a role in the therapeutic mechanism of the drug.

In the present study, we sought to demonstrate the beneficial effect of metformin treatment on arthrofibrosis and the underlying mechanism of this effect. We demonstrated that key glycolytic enzymes were upregulated in human fibrotic joint capsules. On the other hand, metformin was able

to improve knee ROM, reduce capsular fibrosis and thickening, mitigate inflammatory reactions, and downregulate both fibrotic and glycolytic markers in an arthrofibrotic animal model. We also demonstrated that metformin effectively inhibited TGF-β-induced fibroblast activation and that this inhibitory effect was mediated by a metabolic shift of fibroblasts from OXPHOS to aerobic glycolysis. Interestingly, excessive lactate produced by fibroblasts induced M2-like MΦ polarization and diminished inflammatory responses, further alleviating the fibrotic process.

Materials and methods

Patient samples

Shoulder capsule tissue was collected in accordance with our protocol approved by the First Affiliated Hospital of Chongqing Medical University institutional review board (no. 2020-130). Written informed consent was obtained from all participants. Frozen shoulder capsules were collected from patients with primary frozen shoulder undergoing arthroscopic capsular release (n=8; 6 females and 2 males; mean age 55±4 years). The control tissue was obtained from patients undergoing arthroscopic rotator cuff repair without limited passive range of motion (n=8; 6 females and 2 males; mean age 59±3 years). The collected specimens were immediately transferred to 0.9% saline solution and then transferred to 4% paraformaldehyde solution after trimming for follow-up morphological examination. The protocol used in the present study was compliant with the ethical guidelines of the Helsinki Declaration in 1975.

Animal studies

All animal studies were approved by our Institutional Animal Care and Use Committee. Eight-week-old male Sprague Dawley rats with a mean weight of 250 g were used in the present study. Rats were housed in the standard cages (SPF conditions) in a temperature-controlled room with a 12 h light/dark cycle. Twenty rats were divided into four equal groups: control group with only skin incision but no knee immobilization (sham, n=5), immobilized group without intra-articular injection (surgery, n=5), immobilized group injected with an empty vehicle (vehicle, n=5), and immobilized group injected with a metformin-loaded vehicle (metformin, n=5). The vehicle used for intra-articular injections in the present study was PLGA (Sigma-Aldrich, MO, USA). To prepare the metformin-loaded vehicle, PLGA was dissolved in CH_2Cl_2, mixed with metformin dissolved by sonication, and then subjected to a double-emulsion procedure. The preparation protocol and controlled release characteristics of this metformin-loaded PLGA have been described and validated previously (Cheng et al., 2019; Jin et al., 2021).

Immobilization of the right knee was performed by internal fixation of the femur and tibia, as described previously (Abdel et al., 2012; Arsoy et al., 2018; Baranowski et al., 2019; Barlow et al., 2016; Salib et al., 2019; Tibbo et al., 2020). The surgical procedures were performed under general anesthesia with an intraperitoneal injection of ketamine (100 mg/kg) and xylazine (10 mg/kg). After prepping, the knee joint was hyperextended to 45° to disrupt the posterior capsule. Subsequently, a 3 cm long skin incision was made on the anterior surface of the right knee. Muscle bellies adjacent to the mid-diaphysis of the femur and tibia were separated and retracted. Then, a 1-0 Vicryl suture (Ethicon; Johnson & Johnson) was passed several times around both bones and tied to pull the tibia toward the femur, immobilizing the knee joint at 145° flexed position (Suppl-1). Local anesthetic (0.5% ropivacaine) was applied to the surgical site, and the fascial and skin incisions were closed with 4-0 absorbable sutures (Ethicon; Johnson & Johnson). After resuscitation, the animals were left free to move inside the cage. Surgical incisions were observed daily for signs of infection or

inflammation. In addition, abnormal or excessive movement of the immobilized limb, which indicated fixation failure, was also monitored.

Four weeks after the index surgery, the knee fixation sutures of immobilized rats were cut and removed under general anesthesia. Subsequently, 100 μl PLGA or metformin-PLGA suspension (equivalent to 10 mg/kg metformin) was injected into the operated knee joint in the vehicle group or metformin group, respectively. Four weeks later, the ROM of the right knee joint was measured; then, all rats were sacrificed, and the right knee joints were harvested.

Cell culture and chemicals

The NIH3T3 fibroblast cell line was obtained from the Cell Bank of Type Culture Collection of the Chinese Academy of Sciences (Beijing, China) and cultured in Dulbecco's modified Eagle's medium (DMEM, Gibco, Invitrogen, Carlsbad, CA, USA) supplemented with 10% FBS (Gibco) and 1% penicillin-streptomycin (Gibco). All cells were cultured at 37 °C with 5% CO_2 and passaged every 2-3 days upon reaching approximately 90% confluence.

Metformin (Selleck Chemical, S1950, TX, USA) was dissolved in PBS. TGF-β and IFN-γ were purchased from Peprotech (100-21&300-02, NJ, USA). Lactate was purchased from Sigma-Aldrich (867-56-1, MO, USA). Unless indicated otherwise, all chemicals were purchased from Sigma-Aldrich or Corning.

Cell viability

Cell viability was determined by the CCK-8 method (Med Chem Express, Shanghai, China) following the manufacturer's protocol. To assess the toxicity of the dosage, NIH3T3 fibroblasts were treated with a gradient of metformin concentrations (0-8 mM) for 48 h. The OD values were determined at a wavelength of 450 nm. Nonlinear regression analysis was used to calculate the half-maximal inhibitory concentrations (percentage of cell proliferation versus drug concentration).

siRNA transfection

Small interfering RNA targeting LDHA and NC siRNA were chemically synthesized by Tsingke Biotech (Tsingke Biotech, China). Transfection of siRNA at a final concentration of 20 nM was performed using Lipofectamine 3000 (Invitrogen, CA, USA) according to the protocol recommended by the manufacturer.

Cell coculture model

For transwell coculturing, differentiated RAW267.4 macrophages were seeded into a six-well plate and incubated with IFN-γ for 24 h (100ng/ml). Meanwhile, NIH3T3 fibroblasts were seeded into the 0.4μm-pore size Corning transwell inserts (Sigma-Aldrich, #3412, NY, USA) and incubated with or without TGF-β (10ng/ml) and Metformin (2mM) for 24 h. In the next day, NIH3T3 and RAW267.4 cells were cocultured in the same six-well plate for 24 h. In another experimental design, differentiated NIH3T3 fibroblasts were seeded into a six-well plate and incubated with or without TGF-β (10ng/ml) for 24 h. Meanwhile, RAW267.4 macrophages were seeded into the 0.4μm-pore size Corning transwell inserts and incubated with or without IL-4 (100ng/ml) for 24 h. In the next day, NIH3T3 and RAW267.4 cells were cocultured in the same six-well plate for 24 h.

qRT-PCR

Total RNA was extracted from the joint capsule tissues and NIH3T3 cells using TRIZOL reagent (Thermo Fisher Scientific, MA, USA) according to the manufacturer's instructions. Reverse transcription was carried out by using an EvoScript Universal cDNA master reagent kit (Med Chem Express, Shanghai, China). SYBR Green qPCR Master Mix (Med Chem Express, Shanghai, China), cDNA, and the primers were mixed according to the manufacturer's instructions. β-Actin was used

as a reference gene. qRT-PCR was performed in three independent replicates. Sequences of the primers are provided in Suppl-2.

Western blotting

Proteins were extracted from the human capsule samples and NIH3T3 cell cultures using RIPA buffer containing phosphatase and protease inhibitors. Thirty micrograms of protein extract were subsequently used for western blotting according to a standard protocol. Antibodies against GLUT1 (ABclonal, A11727), HK2 (ABclonal, A0994), PFKP (ABclonal, A12160), PKM2 (ABclonal, A16700), α-SMA (ABclonal, A1011), FN1 (ABclonal, A7488), LDHA (ABclonal, A0861), and β-actin (Zen Bio, 200068-8F10) were used. The intensity of the protein bands was analyzed by ImageJ software using β-actin as a reference protein.

Measurement of glucose consumption and lactate production

Glucose and lactate levels were determined as described previously using specific assay kits (Solarbio, BC2235& BC2505, Beijing, China) (Chen et al., 2019). A plate reader was used to meaaure the optical density of the reaction solutions (SAMLFTA, Gen5 software; BioTek Instruments, Winooski, VT, USA).

LC-MS

Mass spectrometry analyses were performed using a high-performance liquid chromatography system (1260 series; Agilent Technologies) and mass spectrometer (Agilent 6460; Agilent Technologies). A 10-cm dish of cultured NIH3T3 cells was collected; 1.5 mL of chloroform/methanol (2:1, v/v) was added and the cells were vortexed for 1 min and centrifuged at 3,000 rpm for 10 minutes; 800 μl of organic phase was added to a clean tube and dried under a flow of nitrogen. Mass spectrometry assay was performed after the addition of 200 μl of isopropanol/methanol solution (1:1, v:v), and the supernatant was used for analysis. Data analyses were performed according to the instructions provided by Shanghai Applied Protein Technology.

Flow cytometry

The markers of RAW264.7 cells were detected using flow cytometry. RAW264.7 cells were seeded at a density of 2×10^6/mL in a 6-well plate. At indicated time points, the cells were digested and collected in 100 μL as cell suspension that was transferred to a flow cytometry tube. Subsequently, cell suspension was incubated with conjugated anti-CD86 and anti-CD206 antibodies (BioLegend, No.105007, 162505, USA) for 30 min at 4 °C in the dark. After washing three times with PBS, the labeled cells were resuspended in 0.2 mL PBS and analyzed using a CytoFLEX system (Beckman Coulter, USA). The data were evaluated by using CytExpert software (Beckman Coulter, USA).

Immunofluorescence assays of the cells

The cells on the coverslips were incubated with 6% normal goat serum and 4% bovine serum albumin in PBS for 1 h at 37 °C. Then, the cells were incubated with anti-FN1 (ABclonal, A7488) and anti-α-SMA antibodies (ABclonal, A1011) overnight at 4 °C. On the next day, fluorescein isothiocyanate (FITC/CY3)-labeled goat anti-rabbit IgG was added as a secondary antibody and incubated for 1 h at room temperature. The stained cells were washed with 1 × PBS 5 times. Finally, the cells were counterstained with DAPI and observed by fluorescence microscopy.

Histological analysis

The samples were fixed in 4% paraformaldehyde (Beyotime, Beijing, China), decalcified in 0.5 M EDTA, and embedded in paraffin. Serial 5-μm-thick sections were obtained and subjected to histological evaluations. HE and Masson's trichrome staining were carried out as described previously (Dai et al., 2020; Liao et al., 2014; Liao et al., 2017). Each specimen was scored by three

orthopedic surgeons following the double-blind principle according to the OARSI criterion for rats (Gerwin, Bendele, Glasson, & Carlson, 2010).

For IHC staining, deparaffinized sections were immersed in sodium citrate buffer, heated in a temperature gradient for antigen retrieval, soaked in 3% H_2O_2 to remove the endogenous peroxidase activity, and blocked with goat serum. Then, the sections were incubated with antibodies against FN1 (ABclonal, A7488), α-SMA (ABclonal, A1011), GLUT1 (ABclonal, A11727), and LDHA (ABclonal, A0861) at 4 °C overnight. A biotin-labeled secondary antibody (ZSGB-BIO, ZLI-9017) and 3,3′-diaminobenzidine (DAB) were used for detection.

Sample size determinations

For *in vitro* experiments quantified as fold changes or by quantitative analysis, we calculated a minimum sample size (n ≥3) based on three independent experiments. For *in vivo* experiments performed similar to previous experiments, we estimated a sample size n ≥ 4 for an alpha level of 0.05 and a power level of 80% (Lazic, Clarke-Williams, & Munafo, 2018; Lin et al., 2021).

Statistical analysis

All datasets were compared using GraphPad Prism (GraphPad Software, La Jolla, CA) version 9.0. The data are shown as the mean ± SEM. For in *vivo* and *vitro* studies, unpaired Student's t test (for two groups) or one-way ANOVA (for multiple groups) followed by the Tukey-Kramer test was used. $P < 0.05$ was considered statistically significant.

Results

Glycolysis is upregulated in human fibrotic capsules

Shoulder adhesive capsulitis is one of the most common forms of arthrofibrosis. Characteristic pathoanatomy of this condition involves contracture of the thickened and stiffened glenohumeral capsule (Fig. 1a). We obtained the samples of the shoulder capsule tissue from patients with or without shoulder adhesive capsulitis during arthroscopic shoulder surgery. As shown in HE sections, the most noticeable changes observed in the fibrotic capsules included the appearance of densely packed collagen fibers, fibroblastic proliferation, and a decrease in subsynovial fat tissue. Increased vascularity and infiltration of inflammatory cells were also detected in the fibrotic tissue but not in nonfibrotic tissue. Similar to these results, Masson's trichrome staining showed significant fibrosis in the fibrotic capsules (Fig. 1b). The results of gene and protein expression analysis demonstrated increased expression of fibrotic markers, including α-SMA, FN1, and TGF-β, in the capsules from adhesive capsulitis patients (Fig. 1c-h). These findings were consistent with previous reports about the pathophysiology of arthrofibrosis (C. H. Cho, Lho, Hwang, & Kim, 2019; Kim et al., 2016; Oki et al., 2015).

Next, we measured the expression of the key glycolytic enzymes to assess whether fibrotic capsules are characterized by upregulated glycolysis compared with the nonfibrotic capsules. The data of qRT-PCR analysis indicated that fibrotic capsules exhibited significantly elevated expression of several rate-limiting glycolytic enzymes, including GLUT1, HK2, PFKFB3, PFKP, PKM, and LDHA (Fig. 1c-d). In agreement with these observations, the data of western blotting showed that the protein expression levels of GLUT1, PFKP, PKM2, and LDHA were significantly upregulated (at least 2-fold) in the fibrotic capsules compared with those in the nonfibrotic capsules (Fig. 1e-f). GLUT1 is responsible for cellular glucose uptake, and abnormal expression of GLUT1 is associated with many disorders (Chen et al., 2019; S. Y. Lee, Abel, & Long, 2018; B. Li et al., 2020). On the other hand, LDHA is critical for the conversion of pyruvate to lactate and dictates the cellular metabolic pathway downstream of glycolysis (W. C. Lee, Guntur, Long, & Rosen, 2017). Thus, we

focused on the expression of GLUT1 and LDHA in the capsule tissues. In agreement with the results of qRT-PCR and western blotting, the data of IHC staining indicated more than twofold increase in both GLUT1 and LDHA positivity in the fibrotic capsules compared with those in the normal capsules (Fig. 1g-h). Overall, our data indicated that glycolysis was upregulated in the human fibrotic capsules.

Metformin alleviates arthrofibrosis in an animal model

We established a knee arthrofibrosis animal model to explore the antifibrotic effect of metformin i*n vivo* (Fig. 2a). As shown in Fig. 2b, the operated knee ROM (extension-flexion) was significantly lower in the surgery group than that in the sham group (-73.0°). No significant differences were detected by comparing the surgery and vehicle groups; however, the ROM of immobilized knees injected with metformin was by 48.6° higher than that of the vehicle-injected knees, indicating that intra-articular metformin injection significantly improved ROM in the arthrofibrotic knees.

We used the synovial membrane histologic inflammation score to examine the type, extent, and severity of inflammation. These properties are based on an increase in the numbers of synovial lining cell layers, proliferation of subsynovial tissue, and infiltration of inflammatory cells (Gerwin et al., 2010). As shown in Fig. 2c, immobilization induced an obvious intra-articular inflammatory reaction, and metformin treatment produced a beneficial anti-inflammatory effect. The results of both HE and Masson staining demonstrated that immobilization surgery led to a decrease in synovial fold and subsynovial fat tissue, prominent capsular thickening, and fibrosis. The vehicle group shared similar histological characteristics with the surgery group; however, the knees of the metformin group were characterized by less severe capsular thickening and fibrosis. In addition, subsynovial fat tissue was more abundant in the metformin group than that in the surgery and vehicle groups (Fig. 2d-e).

α-SMA is expressed by myofibroblasts and smooth muscle cells of the blood vessels and is a marker of both fibrosis and angiogenesis. On the other hand, FN1 is primarily secreted by fibroblasts and myofibroblasts and has been used as a specific marker of fibrosis. On IHC sections, it is found that there were abundant α-SMA-positive and FN1-positive cells at the transition from the capsule to the meniscus (Fig. 3a-b). In the sham group, α-SMA-positive cells covered 11.1% of the capsule area, and in the surgery group, this number was increased to 48.7%. After metformin treatment, the α-SMA-positive area was significantly decreased to 28.4% (Fig. 3a, e). In the case of FN1-positive cells, the area percentage was 4.3% in the sham group, 31.1% in the surgery group, and 12.1% in the metformin group (Fig. 3b, f). We also stained the sections with anti-GLUT1 and anti-LDHA antibodies and examined staining positivity. Similar to the trend observed in the case of α-SMA and FN1, surgery induced a large increase in GLUT1-positive and LDHA-positive areas, and metformin injection significantly reduced the percentages of GLUT1-positive and LDHA-positive cells (Fig. 3c-d, g-h). Overall, these results suggested that metformin improved knee ROM, reduced capsular fibrosis and thickening, mitigated inflammatory reactions, and downregulated both fibrotic and glycolytic markers in an arthrofibrotic animal model.

Metformin inhibits fibroblast activation and induces aerobic glycolysis

To understand the influence of metformin on the biological and metabolic properties of fibroblasts, the NIH3T3 fibroblast cell line was cultured *in vitro*. Based on previous reports and the results of the CCK-8 assays performed in the current study, we decided to use 2 mM metformin for the rest of the study (J. Li et al., 2020) (Suppl-3). The data of the cell immunofluorescence assay demonstrated that TGF-β, which is the most potent profibrotic cytokine, significantly increased the

fluorescence intensity of α-SMA and FN1, and metformin markedly diminished the expression levels of these two fibrotic markers (Fig. 4a-d). These results confirmed the effect of metformin, inducing inhibition of fibroblast activation.

Next, the expression of the key glycolytic enzymes was examined in cultured cells. The protein and mRNA expression levels of the main rate-limiting glycolytic enzymes, including GLUT1, HK2, PFKP, PKM2, and LDHA, were significantly upregulated by TGF-β, suggesting that fibroblast activation was accompanied by increased glycolytic activity. These data were consistent with histological findings obtained in human capsular tissue samples. Interestingly, metformin treatment disrupted the expression of these glycolytic enzymes at both the transcriptional and translational levels (Fig. 4e-g).

To determine the functional relevance of metformin therapy to glucose metabolism, we assayed glucose consumption and lactate production in the fibroblast cell line. TGF-β-treated cells consumed ~80% more glucose than the cells at baseline, and the addition of metformin caused a reduction in glucose consumption of ~25% compared with that in the cells treated with TGF-β alone (Fig. 5a). On the other hand, TGF-β-treated cells produced an increased amount of lactate (~2.5-fold) in the medium, and metformin intervention further promoted lactate production in the context of decreased glucose consumption (Fig. 5b). Consistently, the ratio of lactate production to glucose consumption was the highest in metformin-treated cells (Fig. 5c).

Accumulating evidence indicates that the effect of metformin is linked to altered metabolic pathways (Giaccari, Solini, Frontoni, & Del Prato, 2021; Janzer et al., 2014; Rena, Hardie, & Pearson, 2017; Tang et al., 2021; Yan et al., 2019). Thus, we systematically assessed the metabolomics profile of fibroblasts using LC-MS analysis after culture with TGF-β and metformin (Fig. 5d). Comparison with the cells treated with TGF-β alone indicated that metformin significantly decreased the levels of the main intermediates during the TCA cycle, including citrate, succinate, isocitrate, and fumarate (Fig. 5e-k). In addition, the cellular level of lactate, which is the final product of aerobic glycolysis, was clearly elevated after metformin treatment (Fig. 5l). We also analyzed the ratios of critical metabolites to better understand the alterations in the metabolic pathways. As shown in Fig. 5m-n, metformin treatment led to a significant reduction in the citrate/pyruvate ratio and a significant elevation in the lactate/pyruvate ratio, suggesting that metformin stimulated lactate production and inhibited the OXPHOS pathway. In brief, metformin effectively inhibited TGF-β-induced fibroblast activation and markedly induced a metabolic shift from OXPHOS to aerobic glycolysis in fibroblasts.

Metformin inhibits fibroblast activation in an LDHA-dependent manner

LDHA is critical for metabolic pathway determination between OXPHOS and aerobic glycolysis. To test the importance of LDHA in the antifibrotic effect of metformin, we silenced LDHA in cultured fibroblasts and measured the expression of fibrotic markers. As shown in Fig. 6, siLDHA treatment significantly increased both the mRNA and protein expression levels of α-SMA and FN1 in the cells cultured with metformin, indicating that the inhibitory effect of metformin on fibroblast activation was mediated by metabolic reprogramming of fibroblasts.

Fibroblast-derived lactate induces M2-like MΦ polarization and decreases inflammation

MΦs play an important role in the regulation of the joint microenvironment. We examined whether MΦs were involved in the anti-fibrotic mechanism of metformin. In the fibroblast-MΦ coculture system, metformin-treated fibroblasts significantly reduced the mRNA expression of inflammatory markers, including IL1β, IL6, and TNF-α, in MΦs pretreated with IFN-γ (Fig. 7a-b). In addition,

coculture with metformin-treated fibroblasts markedly enhanced the expression of the M2 MΦ markers Arg-1 and CD163 and significantly decreased the expression of the M1 MΦ marker iNOS (Fig. 7a-b). Next, we treated the IFN-γ-pretreated MΦs with lactate to test if the aforementioned effect was mediated by excessive fibroblast-derived lactate. Quite interestingly, lactate alone exerted the same influence on MΦs as metformin-treated fibroblasts (Fig. 7c-d). Besides, we detected the ratio of $CD86^+$ and $CD206^+$ cells, which are markers of M1- and M2-like MΦ polarization, respectively, by flow cytometry. Lactate treatment led to a decrease in the proportion of $CD86^+$ cells and an increase in the proportion of $CD206^+$ cells (Fig. 7e-i). Lastly, activated fibroblasts were cocultured with M1 or M2 MΦs, respectively (Fig. 7j). As shown in Fig. 7k-o, fibroblasts cocultured with M2 MΦs exhibited significantly less expressions of α-SMA and FN1, at both the transcriptional and translational levels, indicating that M2-like MΦ polarization contributes to the suppression of fibroblast activation. Overall, these results suggested that fibroblast-derived lactate induced M2-like MΦ polarization and diminished the inflammatory reaction, further intercepting fibroblast activation.

Discussion

The present study describes the antifibrotic function of metformin and underlying metabolic reprogramming and anti-inflammatory mechanisms of this effect, providing evidence for the treatment of arthrofibrosis. We demonstrated using both the tissue samples and cell cultures that the strong fibrotic phenotype is accompanied by upregulation of glycolytic capacity in fibroblasts. Treatment with metformin alleviated joint contracture and ECM deposition, mitigated inflammatory reactions, and downregulated both fibrotic and glycolytic markers in a preclinical model of arthrofibrosis. Similarly, metformin reversed the fibrotic response and induced a metabolic shift from OXPHOS to aerobic glycolysis in activated fibroblasts. Subsequently, increased lactate produced by fibroblasts mediated the anti-inflammatory M2-like MΦ polarization, further intercepting the fibrotic process.

Several reports have shown that metformin can prevent and even reverse fibrotic processes in multiple organs, including the kidney, lung, and liver (Feng et al., 2017; Han et al., 2021; Kheirollahi et al., 2019; Li et al., 2021; McCloskey et al., 2020; Mummidi et al., 2016; Rangarajan et al., 2018; Sato et al., 2016; Tang et al., 2021). A recent study confirmed the positive effect of metformin in suppressing joint capsular fibrosis in a mouse model of knee contracture (Tokuda et al., 2021). Previously, the antifibrotic action of metformin was reported to be primarily mediated via AMPK activation and the downstream signaling cascades in fibroblasts, leading to upregulated mitochondrial biogenesis and decreased lactate production (Rangarajan et al., 2018; Tang et al., 2021). However, the mechanism described above is somewhat counterintuitive. Inhibition of Complex I of the respiratory chain by metformin has been shown to induce lactate production and suppress ATP generation, switching the metabolic patterns from OXPHOS to aerobic glycolysis (Giaccari et al., 2021; Rena et al., 2017). Recent metabolomic studies have also shown that metformin decreases the levels of almost all intermediates of the TCA cycle and increases the amount of lactate in an AMPK-independent manner (Janzer et al., 2014; Yan et al., 2019). The results of the current study are consistent with these findings to some extent, revealing that metformin treatment induced metabolic reprogramming toward aerobic glycolysis. The mechanism accounting for these contradictory phenomena remains elusive, implying that the effect of metformin is pleiotropic and highly context-dependent (Giaccari et al., 2021).

The fibroblast-MΦ crosstalk underlying the therapeutic mechanism of metformin for

arthrofibrosis is the novel finding of the present study. Previous similar studies largely focused on the cell-autonomous effect of metformin (Feng et al., 2017; Han et al., 2021; Kheirollahi et al., 2019; Li et al., 2021; McCloskey et al., 2020; Mummidi et al., 2016; Rangarajan et al., 2018; Sato et al., 2016; Tang et al., 2021), while the present study extended the mechanism of action of the drug by providing new evidence that metformin-induced fibroblast metabolic rewiring not only plays a cell-autonomous role but also involves a noncell-autonomous role in the resolution of arthrofibrosis. Metabolite-mediated intercellular communications have been proven to be crucial in the case of cancer and chronic inflammatory diseases (Certo, Tsai, Pucino, Ho, & Mauro, 2021). In contrast, the implications of the cell-to-cell interactions in the pathogenesis of fibrotic disorders and their potential therapeutic applications remain largely unknown (Cui et al., 2021).

Lactate has been considered a waste product of glucose metabolism; however, recently, important roles of lactate in energy production, gluconeogenesis, and immunomodulation have been demonstrated (Brooks, 2018; Caslin, Abebayehu, Pinette, & Ryan, 2021; Hui et al., 2017; Ivashkiv, 2020; Rabinowitz & Enerback, 2020; Vadevoo et al., 2021). The present study demonstrated that upon metformin treatment, fibroblast-secreted lactate acted as a “ready-to-sprout” signal to instruct the polarization of MΦs toward the M2-like phenotype. Thus, fibroblasts shape an anti-inflammatory environment to inhibit myofibroblast transformation and induce fibrosis resolution, and these effects are mediated by the release of lactate. A similar phenomenon has also been recently described in skeletal muscles, where endothelial cell-derived lactate promotes MΦ polarization, leading to improved muscle reperfusion and regeneration (Zhang et al., 2020). These observations suggest that lactate shuttling between various cells is an important, yet underappreciated, mechanism in both normal and pathological states.

Distinct MΦ populations have been suggested to control the initiation, maintenance, and resolution of fibrosis (Braga, Agudelo, & Camara, 2015; Conte, 2021; Trachalaki et al., 2021). Classically activated MΦs (M1) secrete proinflammatory cytokines, including TGF-β, IL-1, and TNF, to trigger fibroblast activation and fibrosis development in multiple organs (Cai et al., 2020; Ogawa, Shichino, Ueha, & Matsushima, 2021; Pradere et al., 2013). In contrast, alternatively activated M2 MΦs produce anti-inflammatory mediators and are important for the resolution of inflammation and prevention of fibrosis (Leslie et al., 2020; Liu, Zhang, Joo, & Sun, 2017; Roehlen, Crouchet, & Baumert, 2020). Our results are consistent with previous reports that M2-like MΦ polarization contributes to the suppression of fibroblast activation.

In conclusion, metformin is a potential treatment alternative for arthrofibrosis, and its antifibrotic effect involves metabolic reprogramming in fibroblasts and lactate-induced M2-like MΦ polarization (Fig. 8).

Figure Captions:

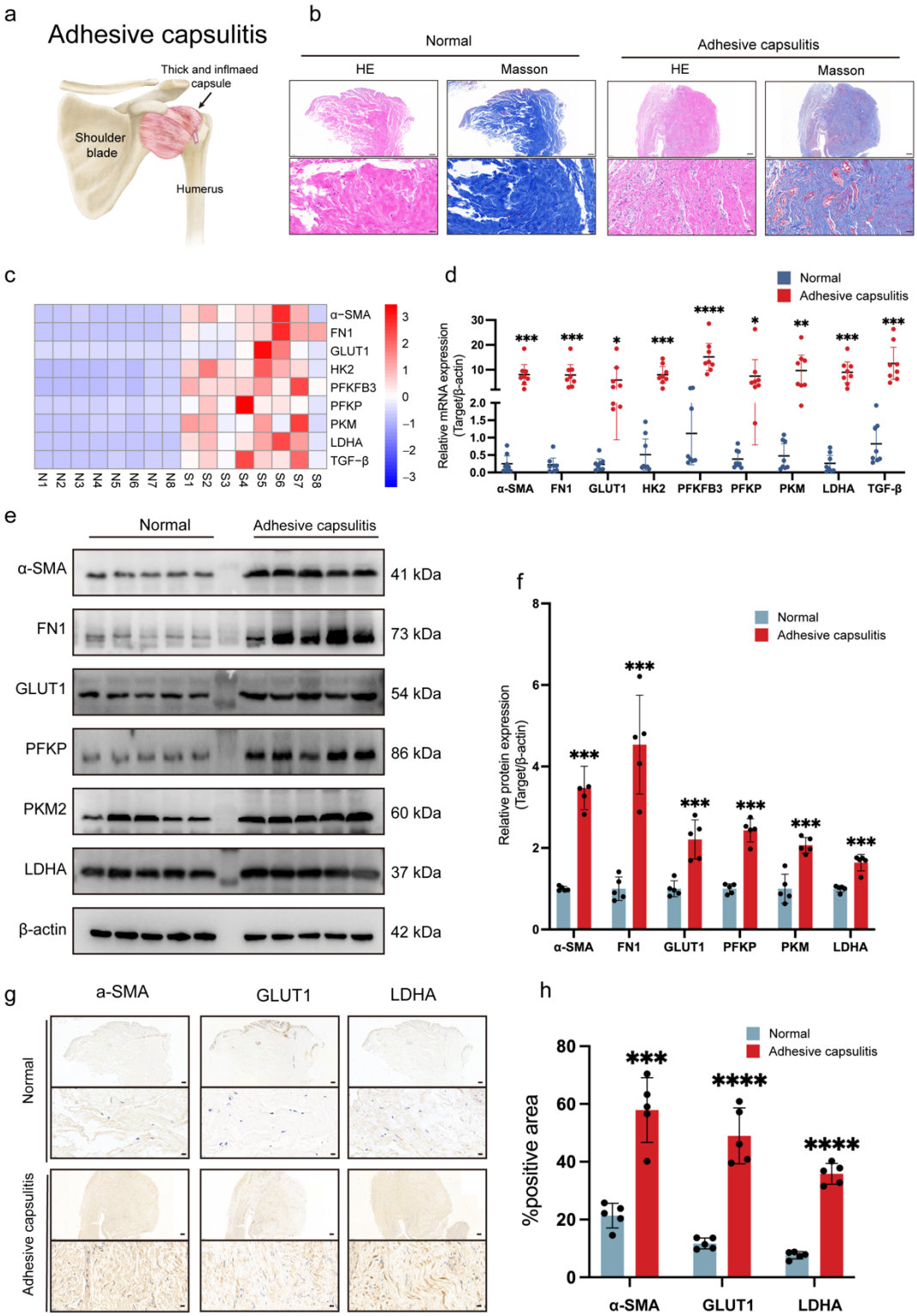

Fig.1 Glycolysis is upregulated in human fibrotic capsules. **a** Schematic illustration of shoulder adhesive capsulitis. **b** The samples of shoulder capsule tissue were obtained from patients with or without shoulder adhesive capsulitis during arthroscopic shoulder surgery and were stained with HE and Masson's trichrome (n=8, scale bars: upper panel: 200 μm, lower panel: 20 μm). Harvested tissues were homogenized, and mRNA (**c-d**) or protein (**e-f**) levels of α-SMA, FN1, TGF-β, GLUT1,

HK2, PFKFB3, PFKP, PKM, and LDHA were quantified by qRT-PCR (n=8) or western blotting (n=5), respectively. The data were normalized to β-actin and expressed as value relative to the level in normal capsular tissue that was designated 1. **g-h** The capsular tissue sections were subjected to IHC staining for α-SMA, GLUT1, and LDHA, and the positive area was quantified (n=5, scale bars: upper panel: 200 μm, lower panel: 10 μm). The data are shown as mean ± SEM. *p<0.05, **p<0.01, ***p<0.001, ****p<0.0001 by unpaired Student's t test.

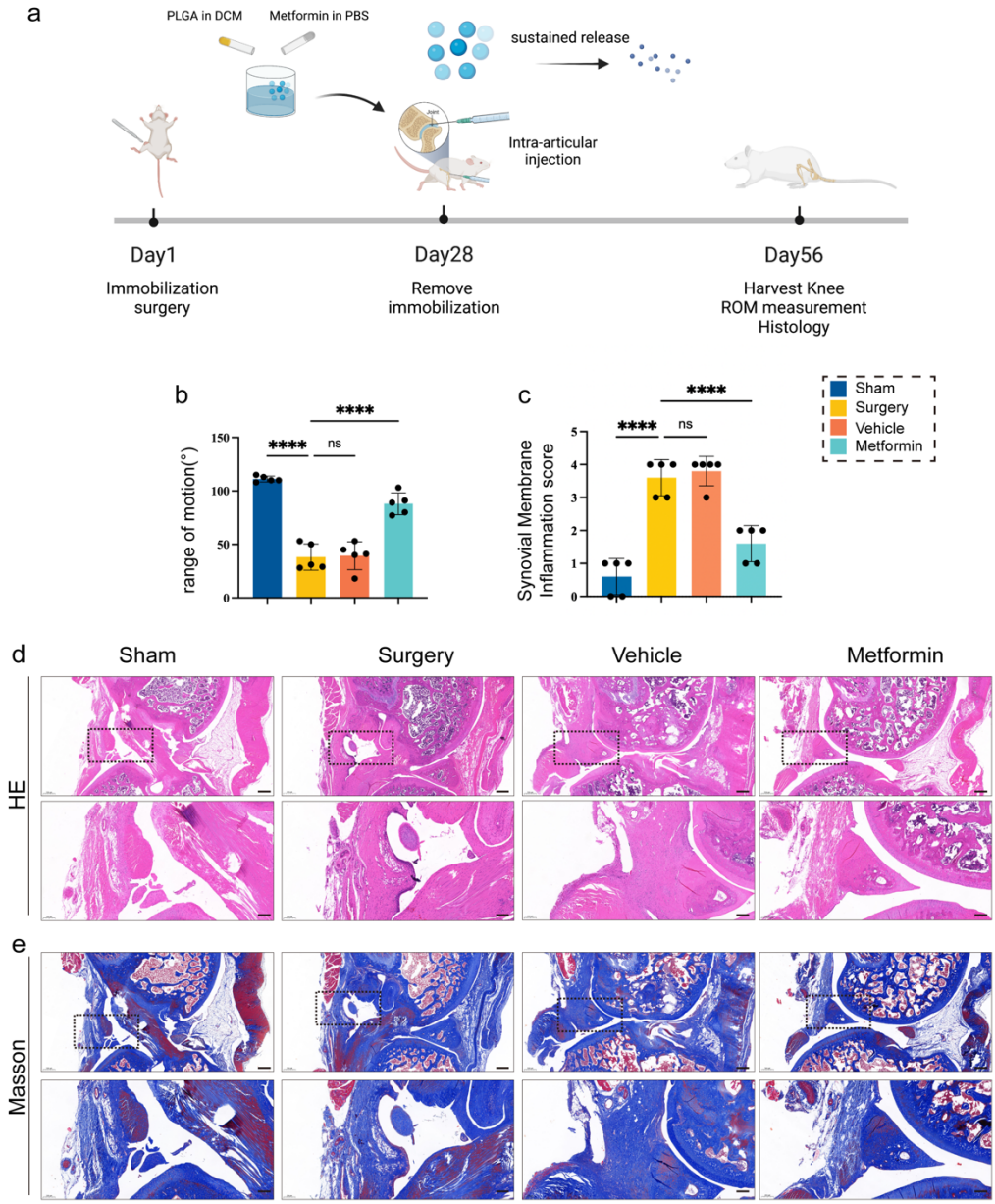

Fig.2 Metformin alleviates arthrofibrosis in animal model. **a** Schematic illustration of the animal study design. Rats were divided into four equal groups: sham, surgery, vehicle, and metformin treatments (n=5). Right knee immobilization surgery was performed on day 1. Four weeks later, the immobilization suture was removed, and metformin or empty vehicle was injected intra-articularly. After four additional weeks, the right knee ROM was measured, rats were euthanized, and the knee was harvested for histological examination. **b** ROM measurement at the endpoint of the study (n=5). **c** Synovial membrane inflammation score assessed using HE sections (n=5). **d-e** Immobilized knees

were stained with HE and Masson's trichrome. The data are shown as mean ± SEM. *p<0.05, **p<0.01, ***p<0.001, ****p<0.0001 by one-way ANOVA followed by Tukey-Kramer test. Scale bars: upper panel: 500 μm, lower panel: 200 μm.

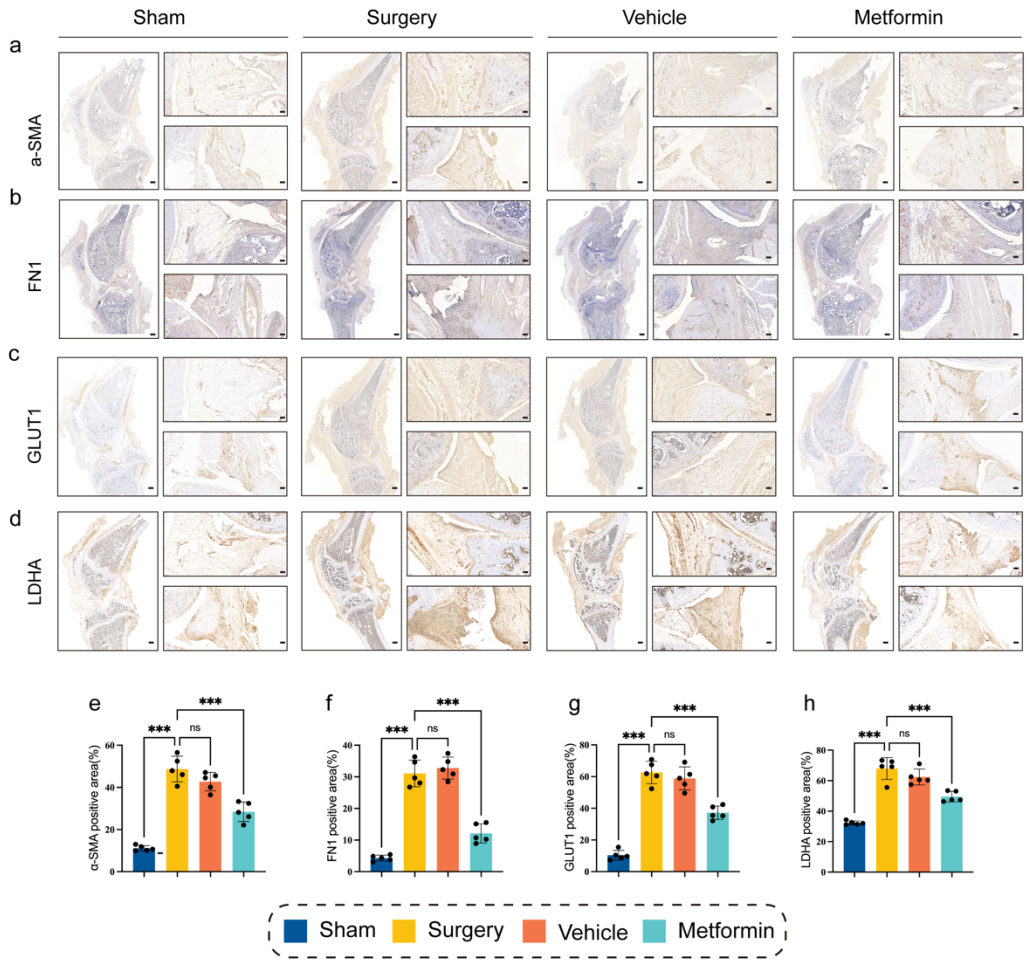

Fig.3 Metformin downregulates both fibrotic and glycolytic markers in an arthrofibrotic animal model. The knee sections of the model animals were subjected to IHC staining for α-SMA, FN1, GLUT1, and LDHA (**a-d**), and the positive area was evaluated (**e-h**). The data are shown as mean ± SEM. *p<0.05, **p<0.01, ***p<0.001, ****p<0.0001 by one-way ANOVA followed by Tukey-Kramer test. Scale bars: left panel: 1000 μm, right panel: 100 μm.

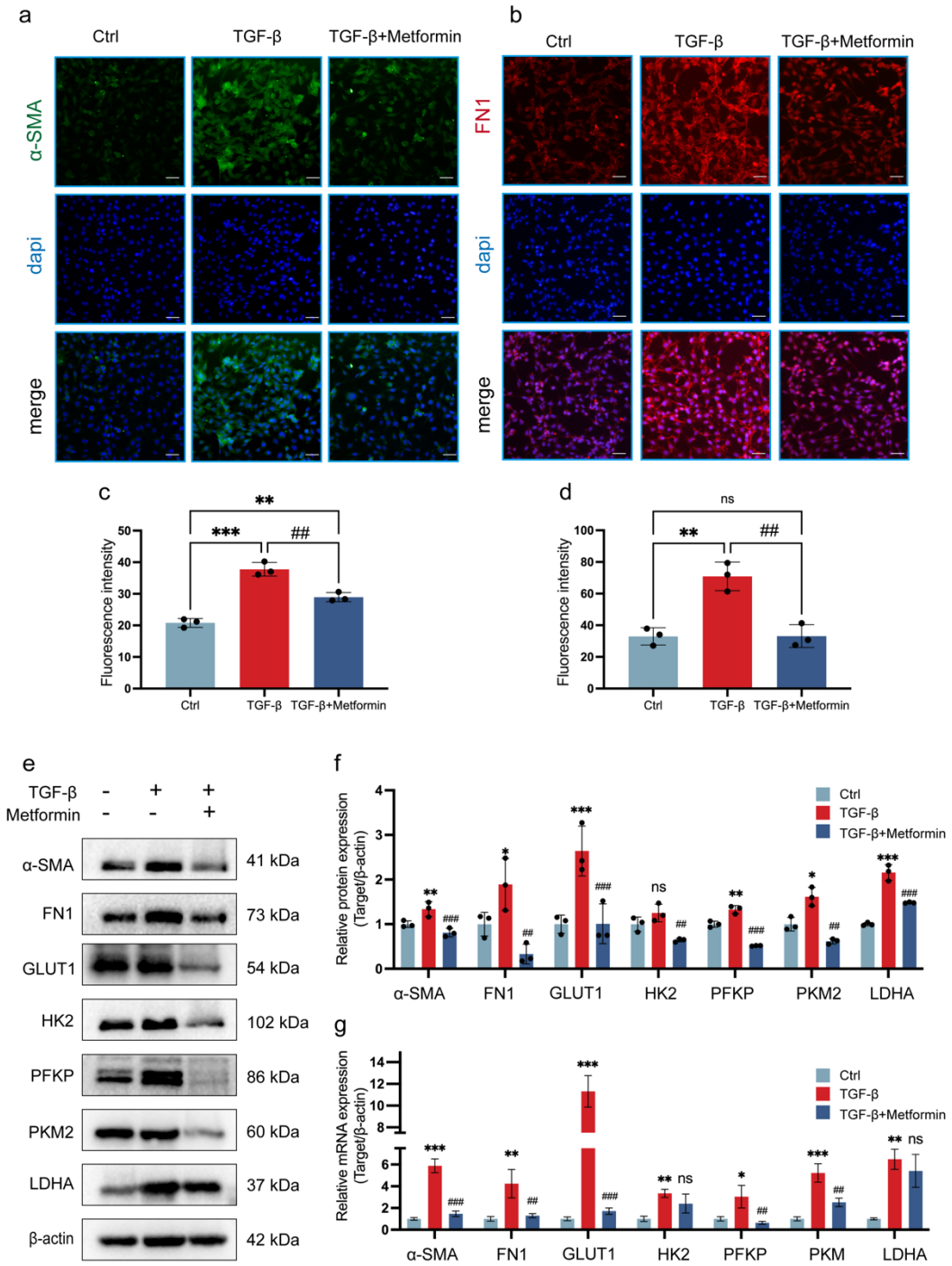

Fig.4 Metformin inhibits fibroblast activation and glycolytic capacity. NIH3T3 fibroblasts were treated with PBS (control), TGF-β (10 ng/ml), or TGF-β (10 ng/ml) + metformin (2 mM) for 48 h. **a-b** Immunofluorescent staining of α-SMA and FN1. **c-d** The results of quantitative analysis showed a significant decrease in α-SMA and FN1 expression in fibroblasts treated with metformin (n=3). **e** The effects of metformin on the protein synthesis of α-SMA, FN1, GLUT1, HK2, PFKP, PKM2, and LDHA. **f** Statistical analysis of protein expression levels shown in (e) (n=3). Protein abundance

was normalized to β-actin and expressed as relative value to the level in control cells that was designated 1. **g** mRNA levels of α-SMA, FN1, GLUT1, HK2, PFKP, PKM, and LDHA were quantified by qRT-PCR (n=3). Data was normalized to β-actin and expressed as value relative to the level in control cells that was designated 1. The data are shown as mean ± SEM. *comparison between control and TGF-β treated cells, #comparison between TGF-β and TGF-β + metformin treated cells. *$p<0.05$, **$p<0.01$, ***$p<0.001$, ****$p<0.0001$ by one-way ANOVA followed by Tukey-Kramer test. Scale bars: 50μm.

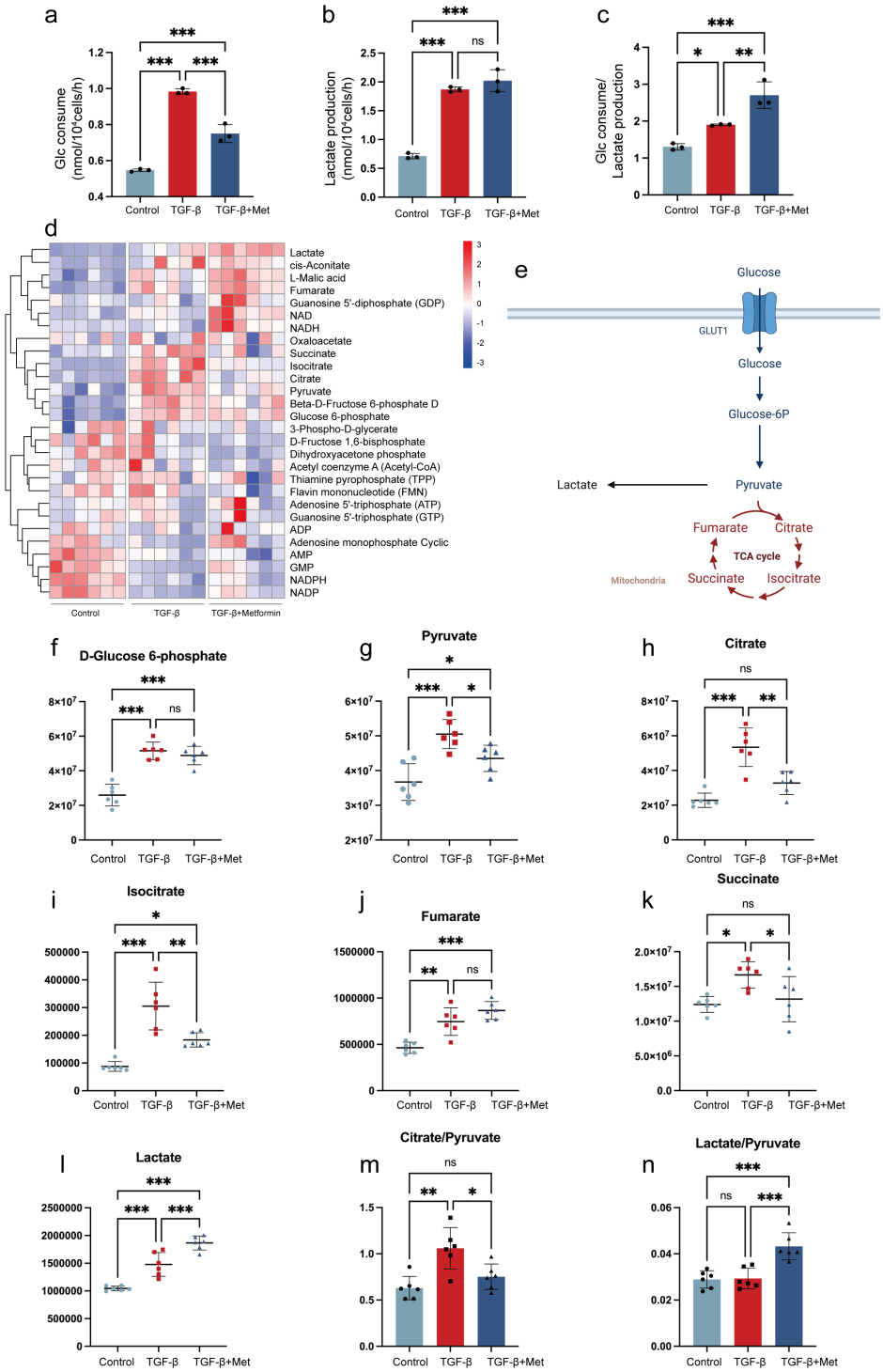

Fig.5 Metformin induces metabolic reprogramming from OXPHOS to aerobic glycolysis in fibroblasts. NIH3T3 fibroblasts were treated with PBS (control), TGF-β (10 ng/ml), or TGF-β (10 ng/ml) + metformin (2 mM) for 48 h. **a-b** Glucose consumption and lactate production by fibroblasts (n=3). **c** The ratio of lactate production to glucose consumption. **d** Heatmap of the main metabolites in control, TGF-β-treated cells, and TGF-β + metformin-treated cells based on LC-MS (n=6). **e** Scheme of the metabolic pathways of aerobic glycolysis and OXPHOS. **f-l** The levels of D-Glucose

6-phosphate, pyruvate, citrate, isocitrate, fumarate, succinate, and lactate in the three groups of cells were compared (n=6). **m-n** Metabolite ratios in differentially treated fibroblasts, including the citrate/pyruvate and lactate/pyruvate ratios (n=6). The data are shown as mean ± SEM. *p<0.05, **p<0.01, ***p<0.001, ****p<0.0001 by one-way ANOVA followed by Tukey-Kramer test.

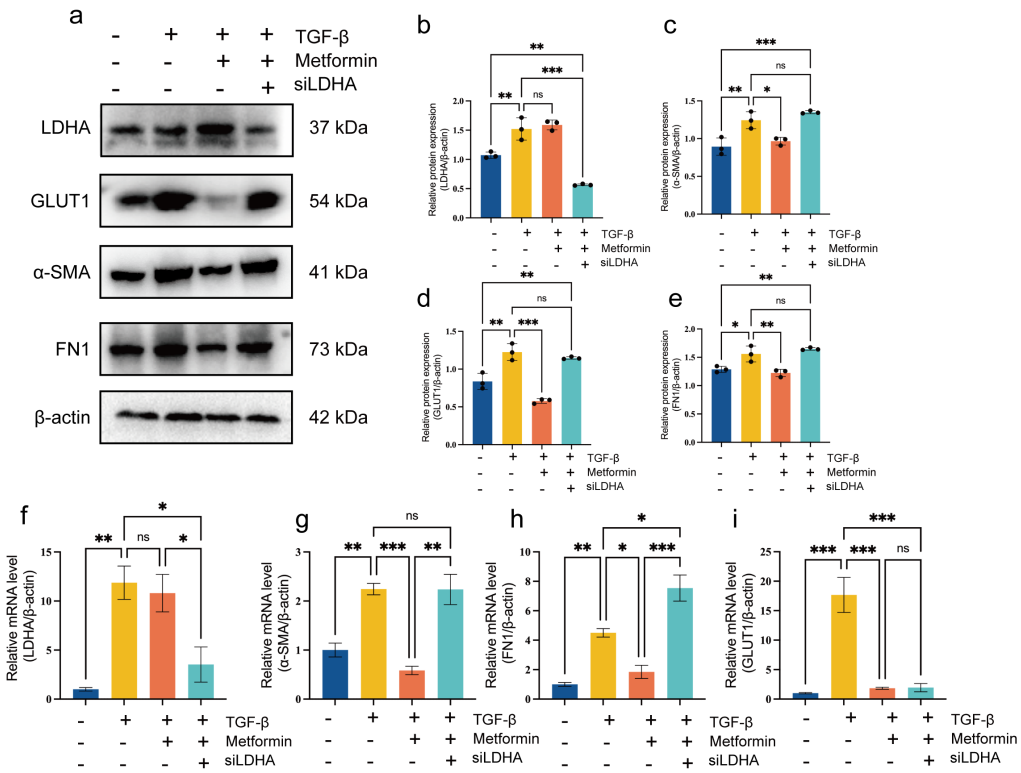

Fig.6 Metformin inhibits fibroblast activation in an LDHA-dependent manner. NIH3T3 fibroblasts were treated with PBS + NC siRNA (control), TGF-β (10 ng/ml) + NC siRNA, TGF-β (10 ng/ml) + metformin (2 mM) + NC siRNA, or TGF-β (10 ng/ml) + metformin (2 mM) + siLDHA for 48 h. **a** Western blot analyses of the total cell lysates of fibroblasts in different groups. **b-e** Statistical analysis of protein expression levels shown in (a) (n=3). Protein abundance was normalized to β-actin and expressed as relative value to the level in control cells that was designated 1. **f-i** mRNA levels of LDHA, α-SMA, FN1, and GLUT1 were quantified by qRT-PCR (n=3). The data were normalized to β-actin and expressed as value relative to the level in control cells that was designated 1. The data are shown as mean ± SEM. *p<0.05, **p<0.01, ***p<0.001, ****p<0.0001 by one-way ANOVA followed by Tukey-Kramer test.

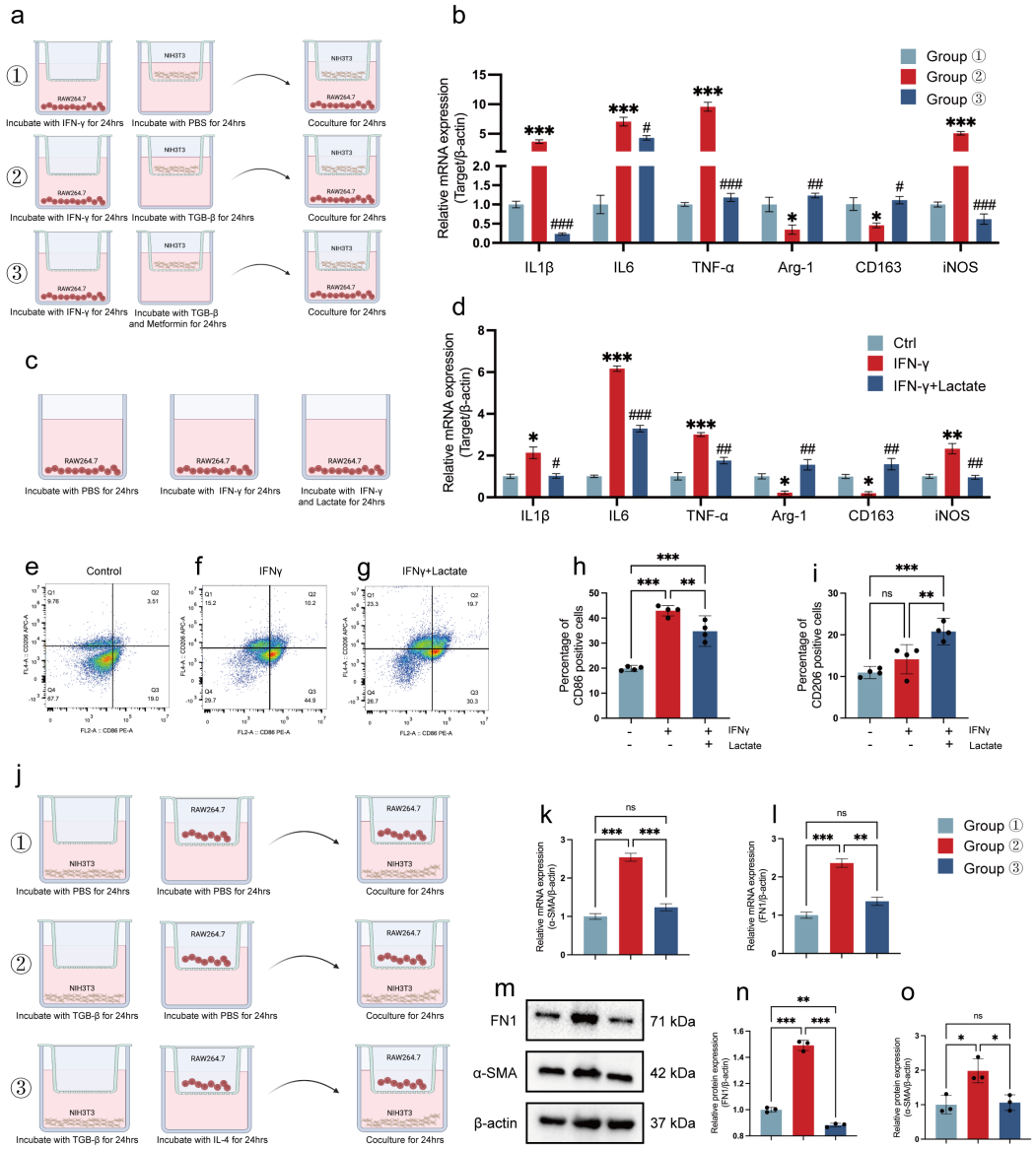

Fig.7 Fibroblast-derived lactate induces M2-like MΦ polarization and decreases inflammation. **a** RAW264.7 cells pretreated with IFN-γ (100 ng/ml) for 24 h were cocultured with NIH3T3 fibroblasts pretreated with either PBS (control), TGF-β (10 ng/ml), or TGF-β (10 ng/ml) + metformin (2 mM) for another 24 h. **b** mRNA levels of IL1β, IL6, TNF-α, Arg-1, CD163, and iNOS were quantified by qRT-PCR (n=3). **c** RAW264.7 cells were treated with either PBS (control), IFN-γ (100 ng/ml), or IFN-γ (100 ng/ml) + lactate (25 mM) for 24 h. **d** mRNA levels of IL1β, IL6, TNF-α, Arg-1, CD163, and iNOS were quantified by qRT-PCR (n=3). **e-g** Representative flow cytometry images detecting CD86+ and CD206+ cells. **h-i** Quantitative results based on (**e-g**) (n=4). **j** NIH3T3 fibroblasts pretreated with PBS (control) or TGF-β (10 ng/ml) for 24 h were cocultured with RAW264.7 cells pretreated with PBS or IL-4 (100 ng/ml) for another 24 h. **k-l** mRNA levels of α-SMA and FN1 were quantified by qRT-PCR (n=3). **m** Representative western blotting images detecting FN1 and α-SMA. **n-o** Statistical analysis of protein expression levels shown in (m) (n=3). Protein abundance was normalized to β-actin and expressed as relative value to the level in control cells that was designated 1. For qRT-PCR, the data were normalized to β-actin and expressed as value relative to the level in control cells that was designated 1. The data are shown as mean ± SEM.

*p<0.05, **p<0.01, ***p<0.001, ****p<0.0001 by one-way ANOVA followed by Tukey-Kramer test.

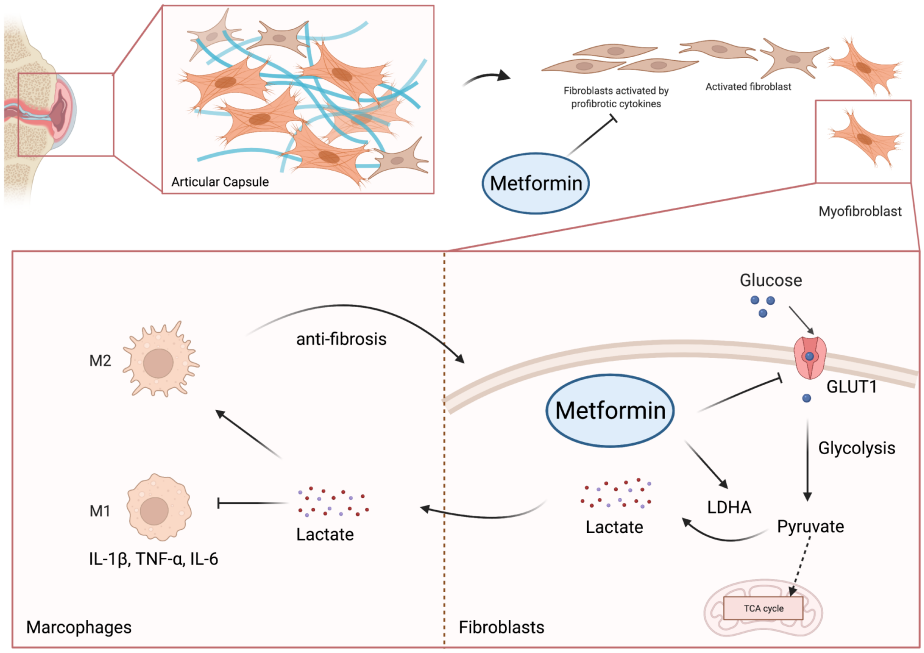

Fig.8 Schematic diagram illustrating the mechanism by which metformin alleviates arthrofibrosis. Metformin inhibits fibroblast activation by inducing a metabolic shift from OXPHOS to aerobic glycolysis in fibroblast. In addition, excessive lactate produced by fibroblasts induces M2-like MΦ polarization and diminishes the inflammatory reaction, further intercepting fibroblast activation.

Descriptive caption for supplementary material:

1 Pictures demonstrating the establishment of arthrofibrotic animal model and intra-articular injection.

2 Primer sequences for qRT-PCR.

3 CCK-8 assay results to test the most suitable concentration of metformin in in vitro study.

Statements & Declarations

Funding This work was supported by Chongqing Natural Science Foundation (Grant No. cstc2019jcyj-msxmX0831), the Science and Technology Research Program of Chongqing Municipal Education Commission (Grant No. KJQN202000430) and Chongqing Medical Scientific Research Project (Grant No. 2021MSXM032). This project was also supported by Innovation Project from Chongqing Municipal Education Commission (#CYB21169) to Z.Z.

Conflict of interest The authors have no relevant financial or non-financial interests to disclose.

Author contributions All authors contributed to the study conception and design. Conceptualization, H.C. and Z.Z.; methodology, Z.Z., S.G., J.Z. and H.Z.; validation, N.H. and W.H.; formal analysis, H.C., X.W. and W.H.; investigation, Z.Z., S.G., H.Z. and Z.C.; resources, H.C., D.W. and W.H.; data curation, Z.Z., S.G. and Y.C.; writing—original draft preparation, H.C., and Z.Z.; writing—review and editing, N.H. and W.H.; supervision, H.C. and W.H.; project administration, H.C., W.H.; funding acquisition, H.C., Z.Z. and W.H. All authors have read and agreed to the published version of the manuscript.

Data availability The datasets generated during and/or analyzed during the current study are available from the corresponding author on reasonable request.

Ethics approval The study was approved by the Ethics Committee of the First Affiliated Hospital of Chongqing Medical University. All animal experiments were performed in accordance with protocols approved by the Animal Care and Use Committee.

Consent to participate Informed consent was obtained from all individual participants included in the study.

Consent to publish No individual information, image or video was included in this study.

References:

Abdel, M. P., Morrey, M. E., Grill, D. E., Kolbert, C. P., An, K. N., Steinmann, S. P., . . . Morrey, B. F. (2012). Effects of joint contracture on the contralateral unoperated limb in a rabbit knee contracture model: a biomechanical and genetic study. *J Orthop Res, 30*(10), 1581-1585. doi:10.1002/jor.22106

Arsoy, D., Salib, C. G., Trousdale, W. H., Tibbo, M. E., Limberg, A. K., Viste, A., . . . Abdel, M. P. (2018). Joint contracture is reduced by intra-articular implantation of rosiglitazone-loaded hydrogels in a rabbit model of arthrofibrosis. *J Orthop Res, 36*(11), 2949-2955. doi:10.1002/jor.24068

Baranowski, A., Schlemmer, L., Forster, K., Slotina, E., Mickan, T., Truffel, S., . . . Rommens, P. M. (2019). Effects of losartan and atorvastatin on the development of early posttraumatic joint stiffness in a rat model. *Drug Des Devel Ther, 13*, 2603-2618. doi:10.2147/DDDT.S204135

Barlow, J. D., Morrey, M. E., Hartzler, R. U., Arsoy, D., Riester, S., van Wijnen, A. J., . . . Abdel, M. P. (2016). Effectiveness of rosiglitazone in reducing flexion contracture in a rabbit model of arthrofibrosis with surgical capsular release: A biomechanical, histological, and genetic analysis. *Bone Joint Res, 5*(1), 11-17. doi:10.1302/2046-3758.51.2000593

Bernard, K., Logsdon, N. J., Ravi, S., Xie, N., Persons, B. P., Rangarajan, S., . . . Thannickal, V. J. (2015). Metabolic Reprogramming Is Required for Myofibroblast Contractility and Differentiation. *J Biol Chem, 290*(42), 25427-25438. doi:10.1074/jbc.M115.646984

Blessing, W. A., Okajima, S. M., Cubria, M. B., Villa-Camacho, J. C., Perez-Viloria, M., Williamson, P. M., . . . Nazarian, A. (2019). Intraarticular injection of relaxin-2 alleviates shoulder arthrofibrosis. *Proc Natl Acad Sci U S A, 116*(25), 12183-12192. doi:10.1073/pnas.1900355116

Braga, T. T., Agudelo, J. S., & Camara, N. O. (2015). Macrophages During the Fibrotic Process: M2 as Friend and Foe. *Front Immunol, 6*, 602. doi:10.3389/fimmu.2015.00602

Brooks, G. A. (2018). The Science and Translation of Lactate Shuttle Theory. *Cell Metab, 27*(4), 757-785. doi:10.1016/j.cmet.2018.03.008

Cai, B., Dongiovanni, P., Corey, K. E., Wang, X., Shmarakov, I. O., Zheng, Z., . . . Tabas, I. (2020). Macrophage MerTK Promotes Liver Fibrosis in Nonalcoholic Steatohepatitis. *Cell Metab, 31*(2), 406-421 e407. doi:10.1016/j.cmet.2019.11.013

Caslin, H. L., Abebayehu, D., Pinette, J. A., & Ryan, J. J. (2021). Lactate Is a Metabolic Mediator That Shapes Immune Cell Fate and Function. *Front Physiol, 12*, 688485. doi:10.3389/fphys.2021.688485

Certo, M., Tsai, C. H., Pucino, V., Ho, P. C., & Mauro, C. (2021). Lactate modulation of immune responses in inflammatory versus tumour microenvironments. *Nat Rev Immunol, 21*(3), 151-161. doi:10.1038/s41577-020-0406-2

Chen, H., Ji, X., Lee, W. C., Shi, Y., Li, B., Abel, E. D., . . . Long, F. (2019). Increased glycolysis mediates Wnt7b-induced bone formation. *FASEB J, 33*(7), 7810-7821. doi:10.1096/fj.201900201RR

Cheng, G., Yin, C., Tu, H., Jiang, S., Wang, Q., Zhou, X., . . . Li, Z. (2019). Controlled Co-delivery of Growth Factors through Layer-by-Layer Assembly of Core-Shell Nanofibers for Improving Bone Regeneration. *ACS Nano, 13*(6), 6372-6382. doi:10.1021/acsnano.8b06032

Cho, C. H., Lho, Y. M., Hwang, I., & Kim, D. H. (2019). Role of matrix metalloproteinases 2 and 9 in the development of frozen shoulder: human data and experimental analysis in a rat contracture model. *J Shoulder Elbow Surg, 28*(7), 1265-1272. doi:10.1016/j.jse.2018.11.072

Cho, S. J., Moon, J. S., Nikahira, K., Yun, H. S., Harris, R., Hong, K. S., . . . Stout-Delgado, H. (2020). GLUT1-dependent glycolysis regulates exacerbation of fibrosis via AIM2 inflammasome

activation. *Thorax, 75*(3), 227-236. doi:10.1136/thoraxjnl-2019-213571

Conte, E. (2021). Targeting monocytes/macrophages in fibrosis and cancer diseases: Therapeutic approaches. *Pharmacol Ther*, 108031. doi:10.1016/j.pharmthera.2021.108031

Cui, H., Xie, N., Banerjee, S., Ge, J., Jiang, D., Dey, T., . . . Liu, G. (2021). Lung Myofibroblasts Promote Macrophage Profibrotic Activity through Lactate-induced Histone Lactylation. *Am J Respir Cell Mol Biol, 64*(1), 115-125. doi:10.1165/rcmb.2020-0360OC

Dai, G., Xiao, H., Zhao, C., Chen, H., Liao, J., & Huang, W. (2020). LncRNA H19 Regulates BMP2-Induced Hypertrophic Differentiation of Mesenchymal Stem Cells by Promoting Runx2 Phosphorylation. *Front Cell Dev Biol, 8*. doi:10.3389/fcell.2020.00580

Feng, Y., Wang, S., Zhang, Y., & Xiao, H. (2017). Metformin attenuates renal fibrosis in both AMPKalpha2-dependent and independent manners. *Clin Exp Pharmacol Physiol, 44*(6), 648-655. doi:10.1111/1440-1681.12748

Gerwin, N., Bendele, A. M., Glasson, S., & Carlson, C. S. (2010). The OARSI histopathology initiative - recommendations for histological assessments of osteoarthritis in the rat. *Osteoarthritis Cartilage, 18 Suppl 3*, S24-34. doi:10.1016/j.joca.2010.05.030

Giaccari, A., Solini, A., Frontoni, S., & Del Prato, S. (2021). Metformin Benefits: Another Example for Alternative Energy Substrate Mechanism? *Diabetes Care, 44*(3), 647-654. doi:10.2337/dc20-1964

Gopu, V., Fan, L., Shetty, R. S., Nagaraja, M. R., & Shetty, S. (2020). Caveolin-1 scaffolding domain peptide regulates glucose metabolism in lung fibrosis. *JCI Insight, 5*(19). doi:10.1172/jci.insight.137969

Hamanaka, R. B., & Mutlu, G. M. (2021). Metabolic requirements of pulmonary fibrosis: role of fibroblast metabolism. *FEBS J*. doi:10.1111/febs.15693

Han, Y. C., Tang, S. Q., Liu, Y. T., Li, A. M., Zhan, M., Yang, M., . . . Yang, S. (2021). AMPK agonist alleviate renal tubulointerstitial fibrosis via activating mitophagy in high fat and streptozotocin induced diabetic mice. *Cell Death Dis, 12*(10), 925. doi:10.1038/s41419-021-04184-8

Henderson, J., Duffy, L., Stratton, R., Ford, D., & O'Reilly, S. (2020). Metabolic reprogramming of glycolysis and glutamine metabolism are key events in myofibroblast transition in systemic sclerosis pathogenesis. *J Cell Mol Med, 24*(23), 14026-14038. doi:10.1111/jcmm.16013

Henderson, N. C., Rieder, F., & Wynn, T. A. (2020). Fibrosis: from mechanisms to medicines. *Nature, 587*(7835), 555-566. doi:10.1038/s41586-020-2938-9

Hui, S., Ghergurovich, J. M., Morscher, R. J., Jang, C., Teng, X., Lu, W., . . . Rabinowitz, J. D. (2017). Glucose feeds the TCA cycle via circulating lactate. *Nature, 551*(7678), 115-118. doi:10.1038/nature24057

Itoi, E., Arce, G., Bain, G. I., Diercks, R. L., Guttmann, D., Imhoff, A. B., . . . Yoo, Y. S. (2016). Shoulder Stiffness: Current Concepts and Concerns. *Arthroscopy, 32*(7), 1402-1414. doi:10.1016/j.arthro.2016.03.024

Ivashkiv, L. B. (2020). The hypoxia-lactate axis tempers inflammation. *Nat Rev Immunol, 20*(2), 85-86. doi:10.1038/s41577-019-0259-8

Janzer, A., German, N. J., Gonzalez-Herrera, K. N., Asara, J. M., Haigis, M. C., & Struhl, K. (2014). Metformin and phenformin deplete tricarboxylic acid cycle and glycolytic intermediates during cell transformation and NTPs in cancer stem cells. *Proc Natl Acad Sci U S A, 111*(29), 10574-10579. doi:10.1073/pnas.1409844111

Jin, S., Xia, X., Huang, J., Yuan, C., Zuo, Y., Li, Y., & Li, J. (2021). Recent advances in PLGA-based

biomaterials for bone tissue regeneration. *Acta Biomater, 127*, 56-79. doi:10.1016/j.actbio.2021.03.067

Kheirollahi, V., Wasnick, R. M., Biasin, V., Vazquez-Armendariz, A. I., Chu, X., Moiseenko, A., . . . El Agha, E. (2019). Metformin induces lipogenic differentiation in myofibroblasts to reverse lung fibrosis. *Nat Commun, 10*(1), 2987. doi:10.1038/s41467-019-10839-0

Kim, D. H., Lee, K. H., Lho, Y. M., Ha, E., Hwang, I., Song, K. S., & Cho, C. H. (2016). Characterization of a frozen shoulder model using immobilization in rats. *J Orthop Surg Res, 11*(1), 160. doi:10.1186/s13018-016-0493-8

Kim du, H., Sung, D. H., Ga, H. Y., & Choi, J. Y. (2014). Metabolic patterns of the shoulder joint on (18)F-fluorodeoxyglucose positron emission tomography/computed tomography in adhesive capsulitis. *Ann Nucl Med, 28*(2), 136-144. doi:10.1007/s12149-013-0794-5

Lazic, S. E., Clarke-Williams, C. J., & Munafo, M. R. (2018). What exactly is 'N' in cell culture and animal experiments? *PLoS Biol, 16*(4), e2005282. doi:10.1371/journal.pbio.2005282

Lee, S. Y., Abel, E. D., & Long, F. (2018). Glucose metabolism induced by Bmp signaling is essential for murine skeletal development. *Nat Commun, 9*(1), 4831. doi:10.1038/s41467-018-07316-5

Lee, W. C., Guntur, A. R., Long, F., & Rosen, C. J. (2017). Energy Metabolism of the Osteoblast: Implications for Osteoporosis. *Endocr Rev, 38*(3), 255-266. doi:10.1210/er.2017-00064

Leslie, J., Macia, M. G., Luli, S., Worrell, J. C., Reilly, W. J., Paish, H. L., . . . Oakley, F. (2020). c-Rel orchestrates energy-dependent epithelial and macrophage reprogramming in fibrosis. *Nat Metab, 2*(11), 1350-1367. doi:10.1038/s42255-020-00306-2

Li, B., Lee, W. C., Song, C., Ye, L., Abel, E. D., & Long, F. (2020). Both aerobic glycolysis and mitochondrial respiration are required for osteoclast differentiation. *FASEB J, 34*(8), 11058-11067. doi:10.1096/fj.202000771R

Li, J., Zhang, B., Liu, W. X., Lu, K., Pan, H., Wang, T., . . . Chen, D. (2020). Metformin limits osteoarthritis development and progression through activation of AMPK signalling. *Ann Rheum Dis, 79*(5), 635-645. doi:10.1136/annrheumdis-2019-216713

Li, S. X., Li, C., Pang, X. R., Zhang, J., Yu, G. C., Yeo, A. J., . . . Peng, C. (2021). Metformin Attenuates Silica-Induced Pulmonary Fibrosis by Activating Autophagy via the AMPK-mTOR Signaling Pathway. *Front Pharmacol, 12*, 719589. doi:10.3389/fphar.2021.719589

Liao, J., Hu, N., Zhou, N., Lin, L., Zhao, C., Yi, S., . . . Huang, W. (2014). Sox9 potentiates BMP2-induced chondrogenic differentiation and inhibits BMP2-induced osteogenic differentiation. *PLoS One, 9*(2), e89025. doi:10.1371/journal.pone.0089025

Liao, J., Yu, X., Hu, X., Fan, J., Wang, J., Zhang, Z., . . . He, T. C. (2017). lncRNA H19 mediates BMP9-induced osteogenic differentiation of mesenchymal stem cells (MSCs) through Notch signaling. *Oncotarget, 8*(32), 53581-53601. doi:10.18632/oncotarget.18655

Lin, X., Wang, W., McDavid, A., Xu, H., Boyce, B. F., & Xing, L. (2021). The E3 ubiquitin ligase Itch limits the progression of post-traumatic osteoarthritis in mice by inhibiting macrophage polarization. *Osteoarthritis Cartilage, 29*(8), 1225-1236. doi:10.1016/j.joca.2021.04.009

Liu, T., Zhang, L., Joo, D., & Sun, S. C. (2017). NF-kappaB signaling in inflammation. *Signal Transduct Target Ther, 2*. doi:10.1038/sigtrans.2017.23

Mattoo, H., & Pillai, S. (2021). Idiopathic pulmonary fibrosis and systemic sclerosis: pathogenic mechanisms and therapeutic interventions. *Cell Mol Life Sci, 78*(14), 5527-5542. doi:10.1007/s00018-021-03874-y

McCloskey, C. W., Cook, D. P., Kelly, B. S., Azzi, F., Allen, C. H., Forsyth, A., . . . Vanderhyden, B. C.

(2020). Metformin Abrogates Age-Associated Ovarian Fibrosis. *Clin Cancer Res, 26*(3), 632-642. doi:10.1158/1078-0432.CCR-19-0603

Mummidi, S., Das, N. A., Carpenter, A. J., Kandikattu, H., Krenz, M., Siebenlist, U., . . . Chandrasekar, B. (2016). Metformin inhibits aldosterone-induced cardiac fibroblast activation, migration and proliferation in vitro, and reverses aldosterone+salt-induced cardiac fibrosis in vivo. *J Mol Cell Cardiol, 98*, 95-102. doi:10.1016/j.yjmcc.2016.07.006

O'Leary, E. M., Tian, Y., Nigdelioglu, R., Witt, L. J., Cetin-Atalay, R., Meliton, A. Y., . . . Hamanaka, R. B. (2020). TGF-beta Promotes Metabolic Reprogramming in Lung Fibroblasts via mTORC1-dependent ATF4 Activation. *Am J Respir Cell Mol Biol, 63*(5), 601-612. doi:10.1165/rcmb.2020-0143OC

Ogawa, T., Shichino, S., Ueha, S., & Matsushima, K. (2021). Macrophages in lung fibrosis. *Int Immunol*. doi:10.1093/intimm/dxab040

Oki, S., Shirasawa, H., Yoda, M., Matsumura, N., Tohmonda, T., Yuasa, K., . . . Horiuchi, K. (2015). Generation and characterization of a novel shoulder contracture mouse model. *J Orthop Res, 33*(11), 1732-1738. doi:10.1002/jor.22943

Phan, T. H. G., Paliogiannis, P., Nasrallah, G. K., Giordo, R., Eid, A. H., Fois, A. G., . . . Pintus, G. (2021). Emerging cellular and molecular determinants of idiopathic pulmonary fibrosis. *Cell Mol Life Sci, 78*(5), 2031-2057. doi:10.1007/s00018-020-03693-7

Pradere, J. P., Kluwe, J., De Minicis, S., Jiao, J. J., Gwak, G. Y., Dapito, D. H., . . . Schwabe, R. F. (2013). Hepatic macrophages but not dendritic cells contribute to liver fibrosis by promoting the survival of activated hepatic stellate cells in mice. *Hepatology, 58*(4), 1461-1473. doi:10.1002/hep.26429

Rabinowitz, J. D., & Enerback, S. (2020). Lactate: the ugly duckling of energy metabolism. *Nat Metab, 2*(7), 566-571. doi:10.1038/s42255-020-0243-4

Rangarajan, S., Bone, N. B., Zmijewska, A. A., Jiang, S., Park, D. W., Bernard, K., . . . Zmijewski, J. W. (2018). Metformin reverses established lung fibrosis in a bleomycin model. *Nat Med, 24*(8), 1121-1127. doi:10.1038/s41591-018-0087-6

Rena, G., Hardie, D. G., & Pearson, E. R. (2017). The mechanisms of action of metformin. *Diabetologia, 60*(9), 1577-1585. doi:10.1007/s00125-017-4342-z

Rockey, D. C., Bell, P. D., & Hill, J. A. (2015). Fibrosis--a common pathway to organ injury and failure. *N Engl J Med, 372*(12), 1138-1149. doi:10.1056/NEJMra1300575

Roehlen, N., Crouchet, E., & Baumert, T. F. (2020). Liver Fibrosis: Mechanistic Concepts and Therapeutic Perspectives. *Cells, 9*(4). doi:10.3390/cells9040875

Salib, C. G., Reina, N., Trousdale, W. H., Limberg, A. K., Tibbo, M. E., Jay, A. G., . . . Abdel, M. P. (2019). Inhibition of COX-2 Pathway as a Potential Prophylaxis Against Arthrofibrogenesis in a Rabbit Model of Joint Contracture. *J Orthop Res, 37*(12), 2609-2620. doi:10.1002/jor.24441

Sato, N., Takasaka, N., Yoshida, M., Tsubouchi, K., Minagawa, S., Araya, J., . . . Kuwano, K. (2016). Metformin attenuates lung fibrosis development via NOX4 suppression. *Respir Res, 17*(1), 107. doi:10.1186/s12931-016-0420-x

Schruf, E., Schroeder, V., Kuttruff, C. A., Weigle, S., Krell, M., Benz, M., . . . Sobotta, M. C. (2019). Human lung fibroblast-to-myofibroblast transformation is not driven by an LDH5-dependent metabolic shift towards aerobic glycolysis. *Respir Res, 20*(1), 87. doi:10.1186/s12931-019-1058-2

Schworer, S., Berisa, M., Violante, S., Qin, W., Zhu, J., Hendrickson, R. C., . . . Thompson, C. B. (2020).

Proline biosynthesis is a vent for TGFbeta-induced mitochondrial redox stress. *EMBO J, 39*(8), e103334. doi:10.15252/embj.2019103334

Selvarajah, B., Azuelos, I., Plate, M., Guillotin, D., Forty, E. J., Contento, G., . . . Chambers, R. C. (2019). mTORC1 amplifies the ATF4-dependent de novo serine-glycine pathway to supply glycine during TGF-beta1-induced collagen biosynthesis. *Sci Signal, 12*(582). doi:10.1126/scisignal.aav3048

Smith-Cortinez, N., van Eunen, K., Heegsma, J., Serna-Salas, S. A., Sydor, S., Bechmann, L. P., . . . Faber, K. N. (2020). Simultaneous Induction of Glycolysis and Oxidative Phosphorylation during Activation of Hepatic Stellate Cells Reveals Novel Mitochondrial Targets to Treat Liver Fibrosis. *Cells, 9*(11). doi:10.3390/cells9112456

Tang, C. J., Xu, J., Ye, H. Y., & Wang, X. B. (2021). Metformin prevents PFKFB3-related aerobic glycolysis from enhancing collagen synthesis in lung fibroblasts by regulating AMPK/mTOR pathway. *Exp Ther Med, 21*(6), 581. doi:10.3892/etm.2021.10013

Tibbo, M. E., Limberg, A. K., Salib, C. G., Turner, T. W., McLaury, A. R., Jay, A. G., . . . Abdel, M. P. (2020). Anti-fibrotic effects of the antihistamine ketotifen in a rabbit model of arthrofibrosis. *Bone Joint Res, 9*(6), 302-310. doi:10.1302/2046-3758.96.BJR-2019-0272.R2

Tokuda, K., Yamanaka, Y., Mano, Y., Tsukamoto, M., Tajima, T., Suzuki, H., . . . Sakai, A. (2021). Effect of metformin treatment and its time of administration on joint capsular fibrosis induced by mouse knee immobilization. *Sci Rep, 11*(1), 17978. doi:10.1038/s41598-021-97445-7

Trachalaki, A., Tsitoura, E., Mastrodimou, S., Invernizzi, R., Vasarmidi, E., Bibaki, E., . . . Antoniou, K. (2021). Enhanced IL-1beta Release Following NLRP3 and AIM2 Inflammasome Stimulation Is Linked to mtROS in Airway Macrophages in Pulmonary Fibrosis. *Front Immunol, 12*, 661811. doi:10.3389/fimmu.2021.661811

Tsuchida, T., & Friedman, S. L. (2017). Mechanisms of hepatic stellate cell activation. *Nat Rev Gastroenterol Hepatol, 14*(7), 397-411. doi:10.1038/nrgastro.2017.38

Usher, K. M., Zhu, S., Mavropalias, G., Carrino, J. A., Zhao, J., & Xu, J. (2019). Pathological mechanisms and therapeutic outlooks for arthrofibrosis. *Bone Res, 7*, 9. doi:10.1038/s41413-019-0047-x

Vadevoo, S. M. P., Gunassekaran, G. R., Lee, C., Lee, N., Lee, J., Chae, S., . . . Lee, B. (2021). The macrophage odorant receptor Olfr78 mediates the lactate-induced M2 phenotype of tumor-associated macrophages. *Proc Natl Acad Sci U S A, 118*(37). doi:10.1073/pnas.2102434118

Won, K. S., Kim, D. H., Sung, D. H., Song, B. I., Kim, H. W., Song, K. S., . . . Cho, C. H. (2017). Clinical correlation of metabolic parameters on (18)F-FDG PET/CT in idiopathic frozen shoulder. *Ann Nucl Med, 31*(3), 211-217. doi:10.1007/s12149-016-1147-y

Xie, N., Tan, Z., Banerjee, S., Cui, H., Ge, J., Liu, R. M., . . . Liu, G. (2015). Glycolytic Reprogramming in Myofibroblast Differentiation and Lung Fibrosis. *Am J Respir Crit Care Med, 192*(12), 1462-1474. doi:10.1164/rccm.201504-0780OC

Yan, M., Qi, H., Xia, T., Zhao, X., Wang, W., Wang, Z., . . . Piao, H. L. (2019). Metabolomics profiling of metformin-mediated metabolic reprogramming bypassing AMPKalpha. *Metabolism, 91*, 18-29. doi:10.1016/j.metabol.2018.11.010

Zhang, J., Muri, J., Fitzgerald, G., Gorski, T., Gianni-Barrera, R., Masschelein, E., . . . De Bock, K. (2020). Endothelial Lactate Controls Muscle Regeneration from Ischemia by Inducing M2-like Macrophage Polarization. *Cell Metab, 31*(6), 1136-1153 e1137. doi:10.1016/j.cmet.2020.05.004

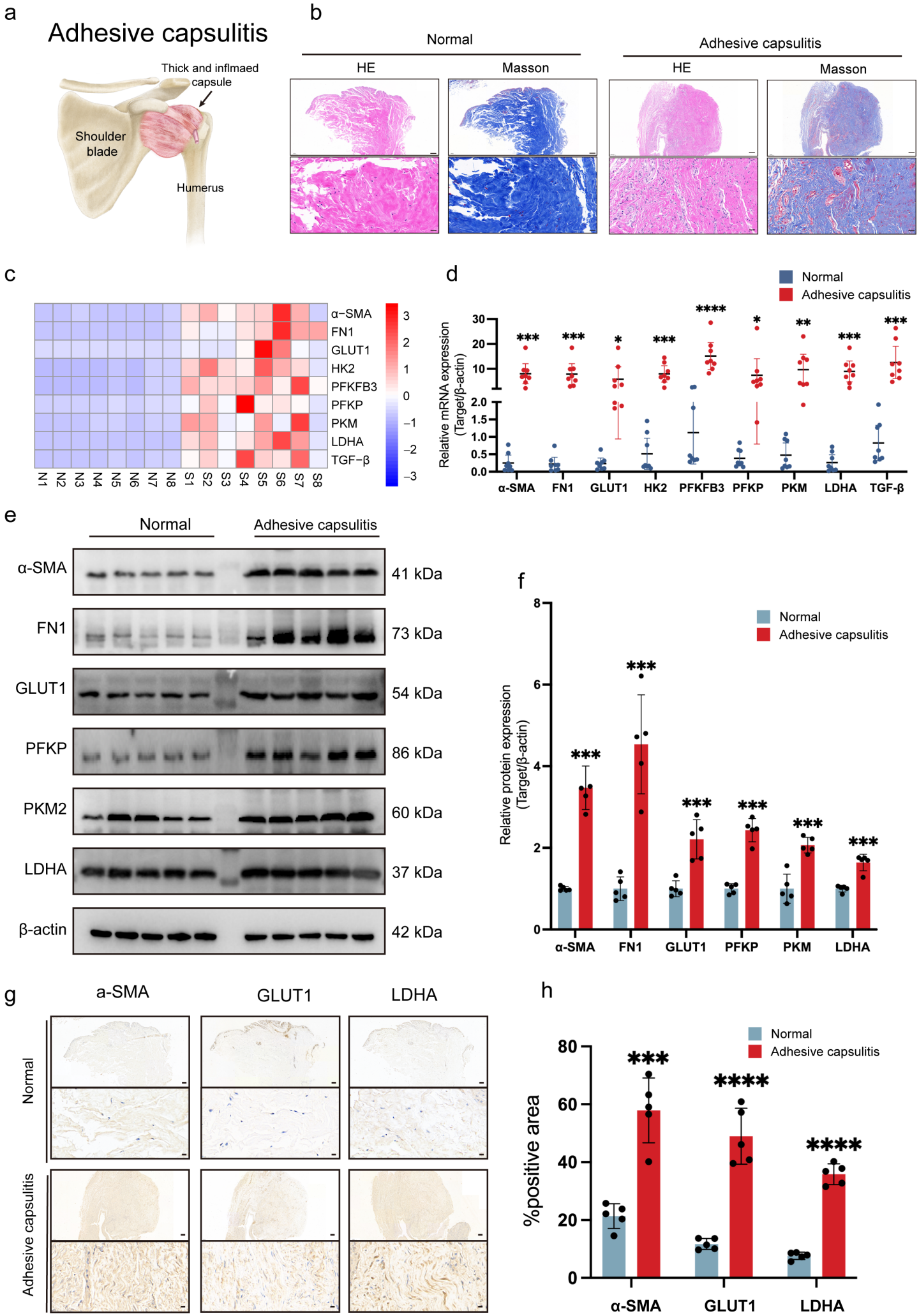
a
Adhesive capsulitis
Thick and inflmaed capsule
Shoulder blade
Humerus
b
Normal
Adhesive capsulitis
HE
Masson
HE
Masson
c
α−SMA
FN1
GLUT1
HK2
PFKFB3
PFKP
PKM
LDHA
TGF−β
N1 N2 N3 N4 N5 N6 N7 N8 S1 S2 S3 S4 S5 S6 S7 S8
3 2 1 0 −1 −2 −3
d
Normal
Adhesive capsulitis
Relative mRNA expression (Target/β-actin)
α-SMA FN1 GLUT1 HK2 PFKFB3 PFKP PKM LDHA TGF-β
e
Normal
Adhesive capsulitis
α-SMA 41 kDa
FN1 73 kDa
GLUT1 54 kDa
PFKP 86 kDa
PKM2 60 kDa
LDHA 37 kDa
β-actin 42 kDa
f
Normal
Adhesive capsulitis
Relative protein expression (Target/β-actin)
α-SMA FN1 GLUT1 PFKP PKM LDHA
g
a-SMA
GLUT1
LDHA
Normal
Adhesive capsulitis
h
Normal
Adhesive capsulitis
%positive area
α-SMA GLUT1 LDHA

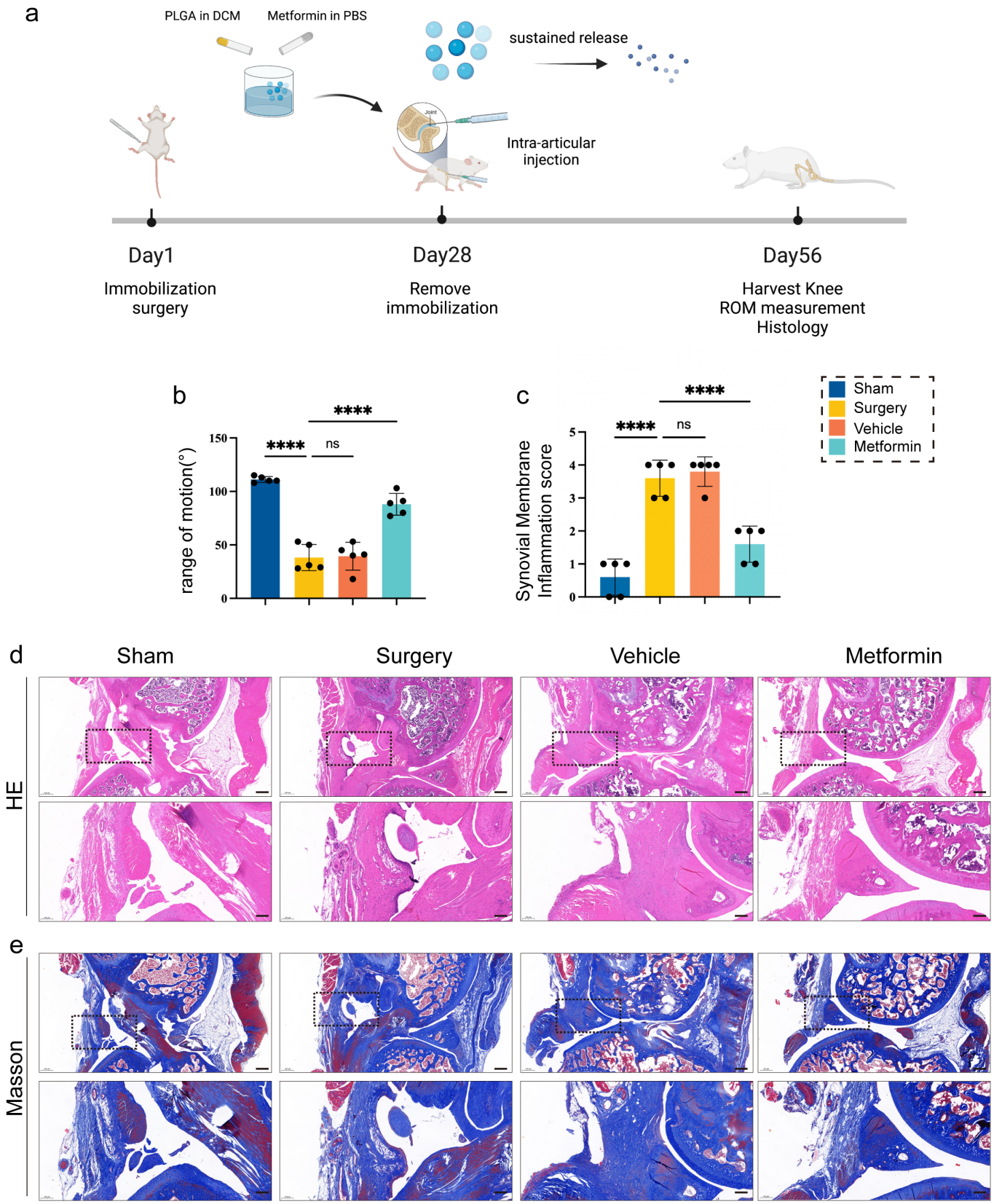
a
PLGA in DCM
Metformin in PBS
sustained release
Intra-articular injection
Day1
Immobilization surgery
Day28
Remove immobilization
Day56
Harvest Knee
ROM measurement
Histology
b
range of motion(°)
****
ns
****
c
Synovial Membrane Inflammation score
****
ns
****
Sham
Surgery
Vehicle
Metformin
d
Sham
Surgery
Vehicle
Metformin
HE
e
Masson

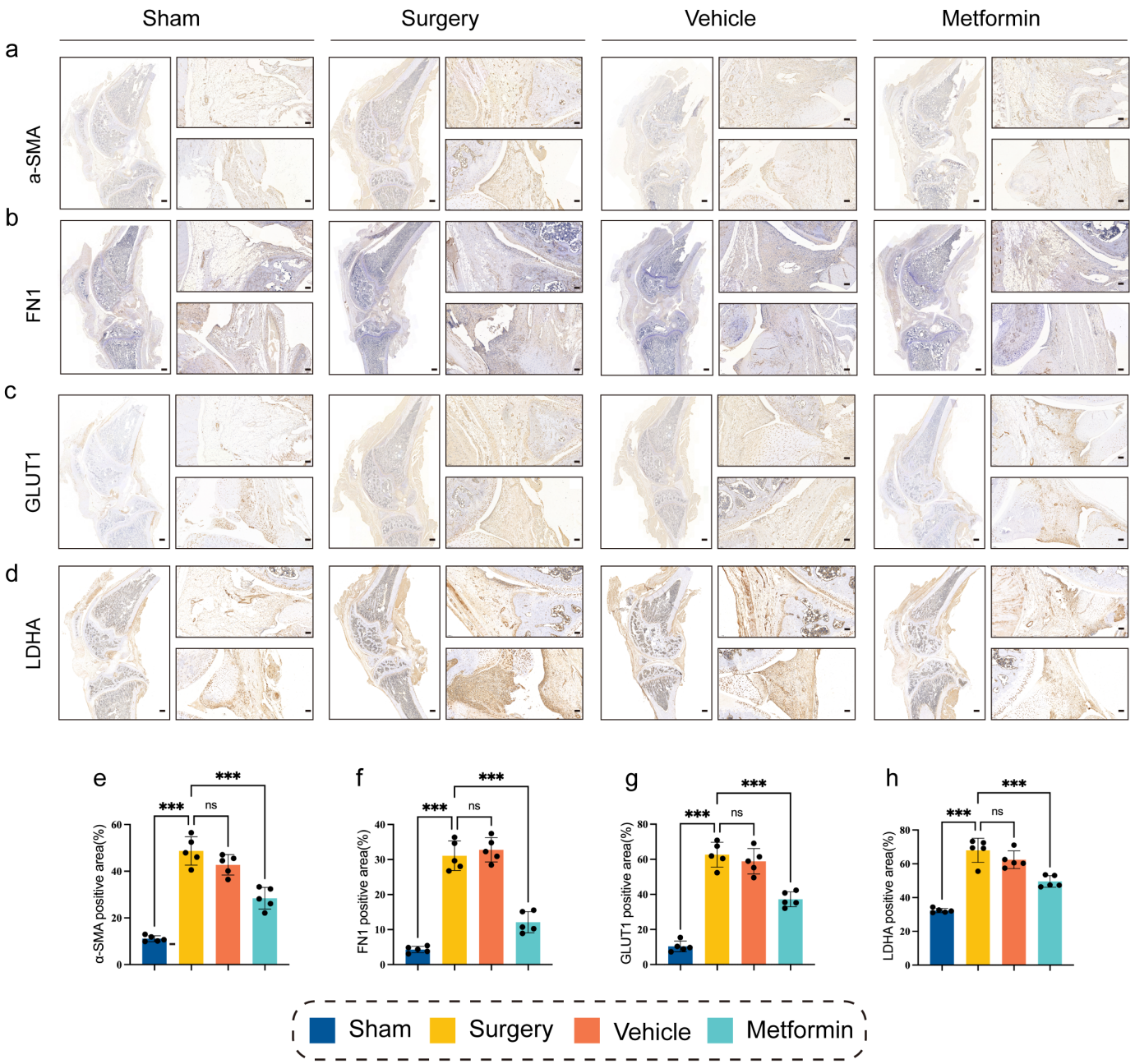
Sham
Surgery
Vehicle
Metformin
a
a-SMA
b
FN1
c
GLUT1
d
LDHA
e
α-SMA positive area(%)
f
FN1 positive area(%)
g
GLUT1 positive area(%)
h
LDHA positive area(%)
***
ns
Sham
Surgery
Vehicle
Metformin

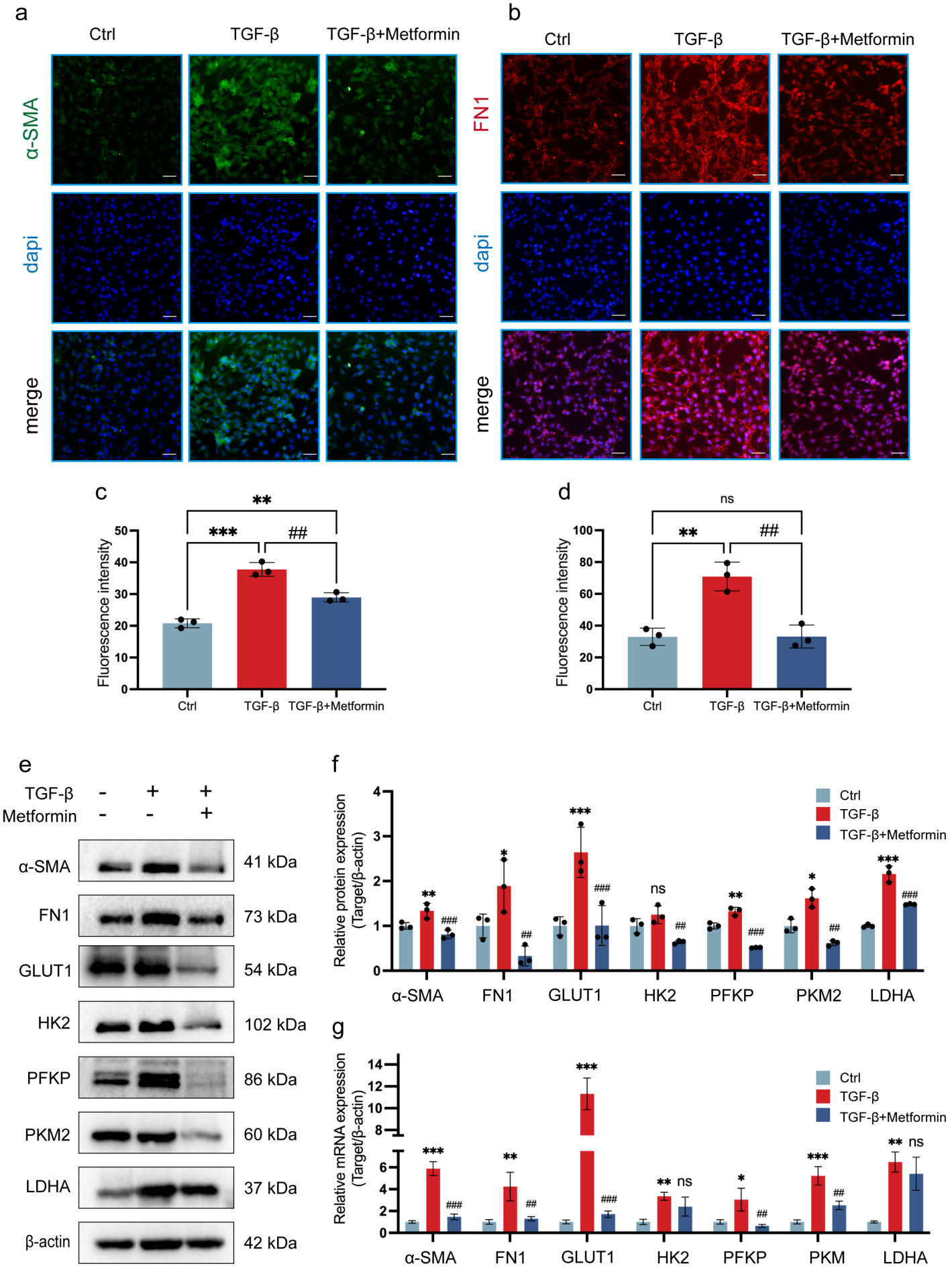
a
Ctrl
TGF-β
TGF-β+Metformin
α-SMA
dapi
merge
b
FN1
c
Fluorescence intensity
d
ns
e
TGF-β
Metformin
41 kDa
73 kDa
54 kDa
102 kDa
86 kDa
60 kDa
37 kDa
42 kDa
f
Relative protein expression (Target/β-actin)
HK2
PFKP
PKM2
LDHA
g
Relative mRNA expression (Target/β-actin)
PKM

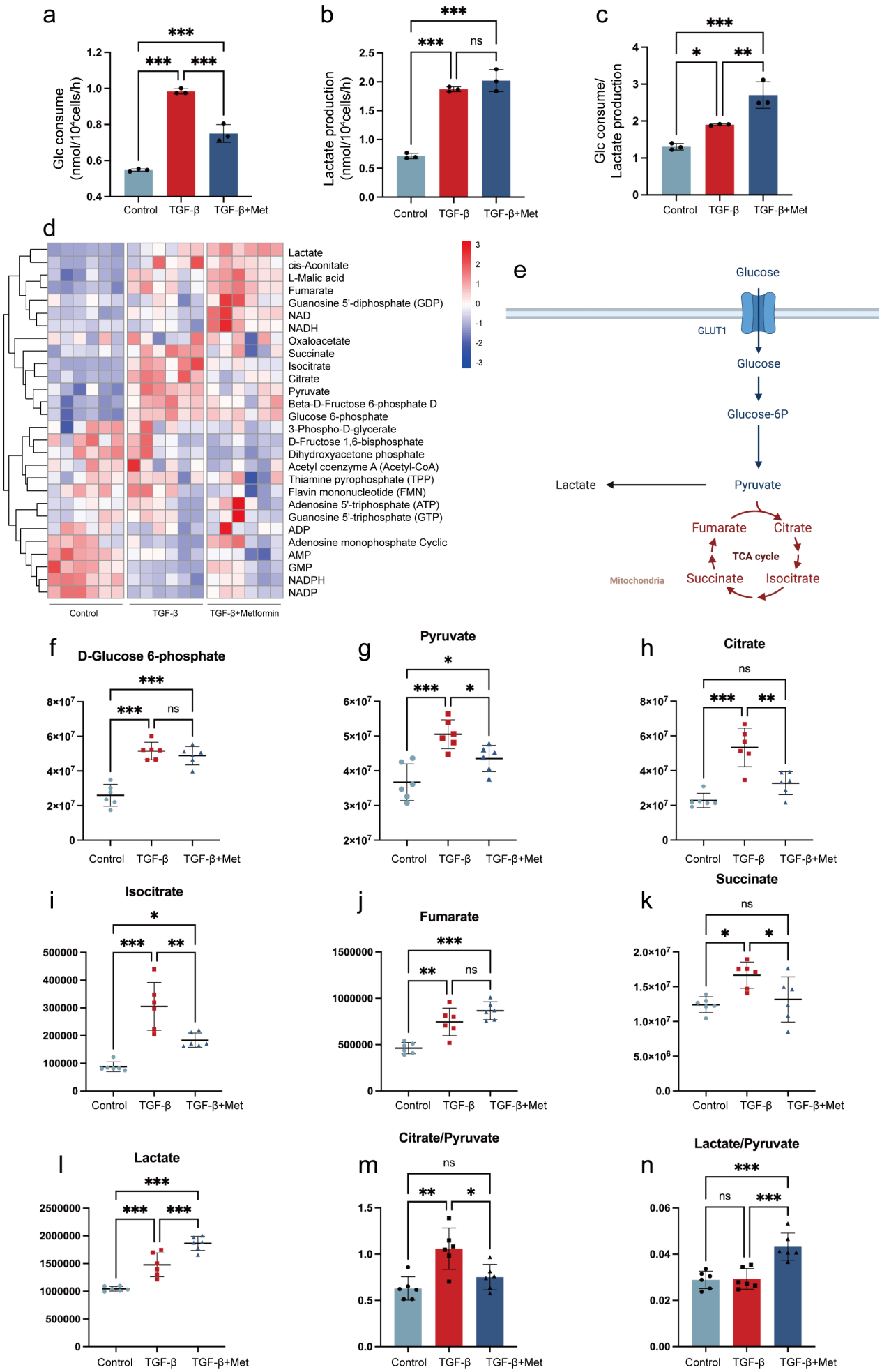
a
Glc consume (nmol/10⁴cells/h)
Control
TGF-β
TGF-β+Met
b
Lactate production (nmol/10⁴cells/h)
ns
c
Glc consume/ Lactate production
d
Lactate
cis-Aconitate
L-Malic acid
Fumarate
Guanosine 5'-diphosphate (GDP)
NAD
NADH
Oxaloacetate
Succinate
Isocitrate
Citrate
Pyruvate
Beta-D-Fructose 6-phosphate D
Glucose 6-phosphate
3-Phospho-D-glycerate
D-Fructose 1,6-bisphosphate
Dihydroxyacetone phosphate
Acetyl coenzyme A (Acetyl-CoA)
Thiamine pyrophosphate (TPP)
Flavin mononucleotide (FMN)
Adenosine 5'-triphosphate (ATP)
Guanosine 5'-triphosphate (GTP)
ADP
Adenosine monophosphate Cyclic
AMP
GMP
NADPH
NADP
TGF-β+Metformin
e
Glucose
GLUT1
Glucose-6P
Pyruvate
Lactate
Fumarate
Citrate
TCA cycle
Succinate
Isocitrate
Mitochondria
f
D-Glucose 6-phosphate
g
Pyruvate
h
Citrate
i
Isocitrate
j
Fumarate
k
Succinate
l
Lactate
m
Citrate/Pyruvate
n
Lactate/Pyruvate

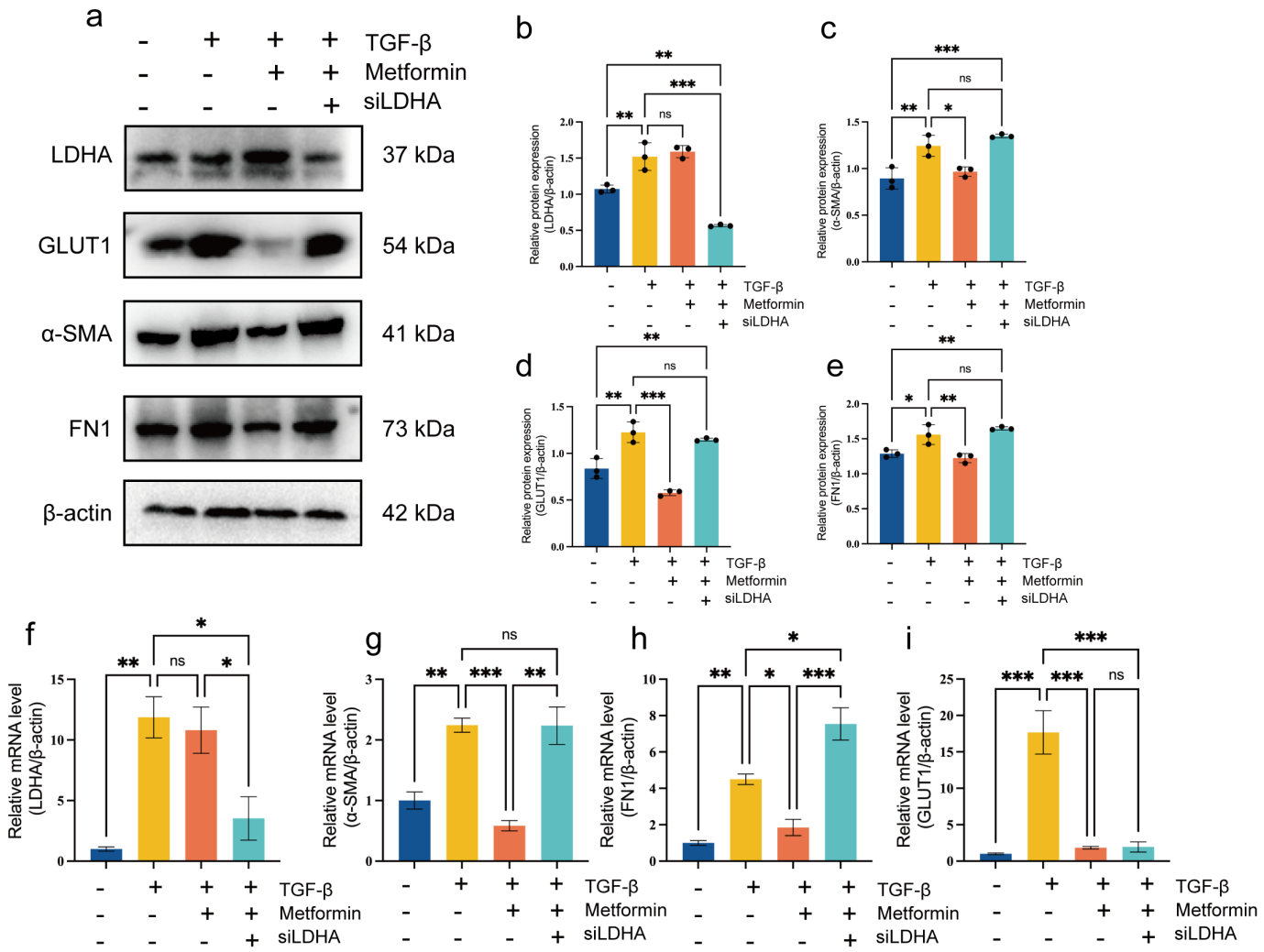
a
TGF-β
Metformin
siLDHA
LDHA
37 kDa
GLUT1
54 kDa
α-SMA
41 kDa
FN1
73 kDa
β-actin
42 kDa
b
Relative protein expression (LDHA/β-actin)
c
Relative protein expression (α-SMA/β-actin)
d
Relative protein expression (GLUT1/β-actin)
e
Relative protein expression (FN1/β-actin)
f
Relative mRNA level (LDHA/β-actin)
g
Relative mRNA level (α-SMA/β-actin)
h
Relative mRNA level (FN1/β-actin)
i
Relative mRNA level (GLUT1/β-actin)
ns

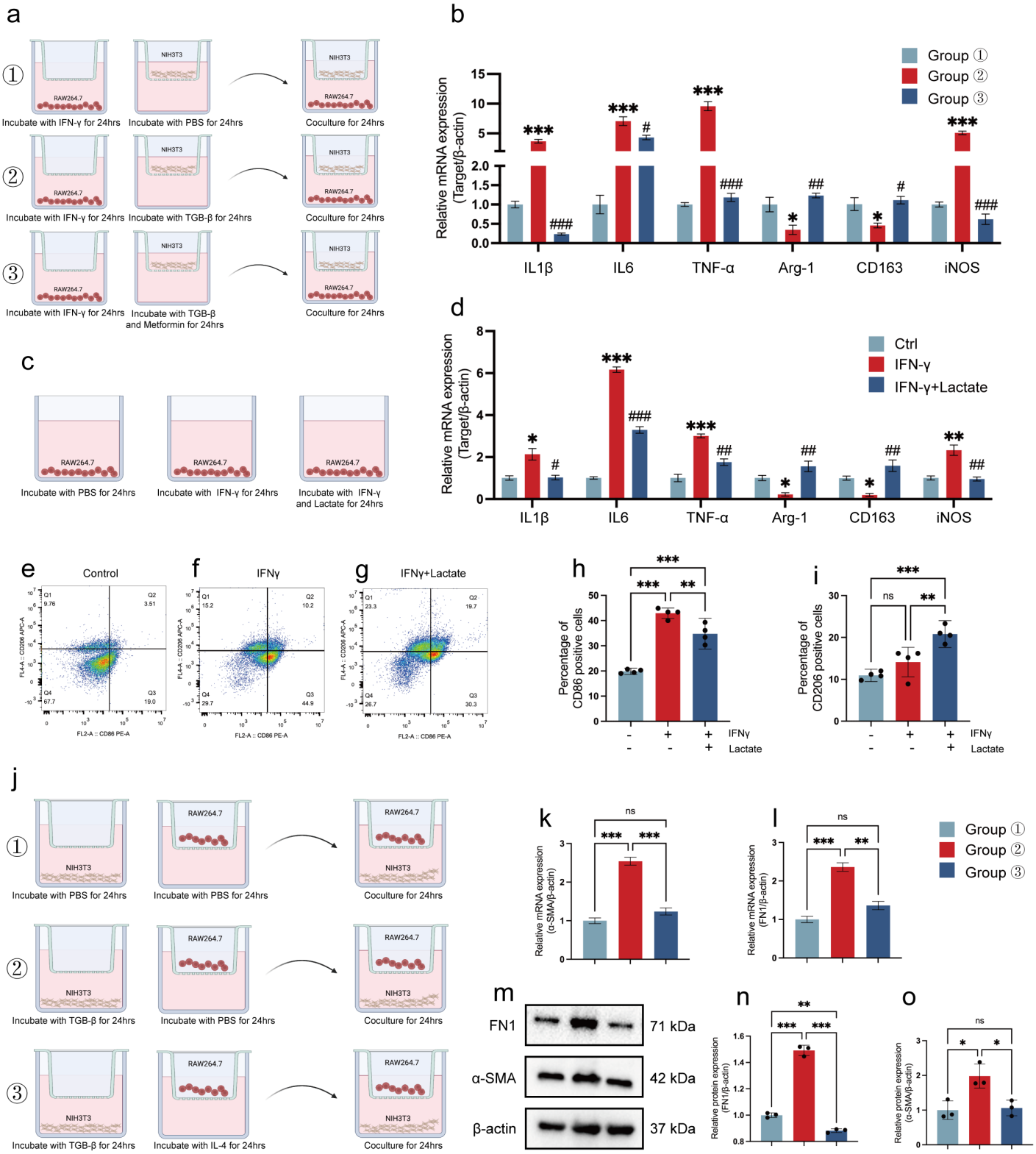
a
①
RAW264.7
Incubate with IFN-γ for 24hrs
NIH3T3
Incubate with PBS for 24hrs
Coculture for 24hrs
②
Incubate with IFN-γ for 24hrs
Incubate with TGB-β for 24hrs
Coculture for 24hrs
③
Incubate with IFN-γ for 24hrs
Incubate with TGB-β and Metformin for 24hrs
Coculture for 24hrs
b
Group ①
Group ②
Group ③
Relative mRNA expression (Target/β-actin)
IL1β
IL6
TNF-α
Arg-1
CD163
iNOS
c
Incubate with PBS for 24hrs
Incubate with IFN-γ for 24hrs
Incubate with IFN-γ and Lactate for 24hrs
d
Ctrl
IFN-γ
IFN-γ+Lactate
e
Control
f
IFNγ
g
IFNγ+Lactate
FL2-A :: CD86 PE-A
FL4-A :: CD206 APC-A
h
Percentage of CD86 positive cells
IFNγ
Lactate
i
Percentage of CD206 positive cells
ns
j
Incubate with TGB-β for 24hrs
Incubate with IL-4 for 24hrs
k
Relative mRNA expression (α-SMA/β-actin)
l
Relative mRNA expression (FN1/β-actin)
m
FN1
71 kDa
α-SMA
42 kDa
β-actin
37 kDa
n
Relative protein expression (FN1/β-actin)
o
Relative protein expression (α-SMA/β-actin)

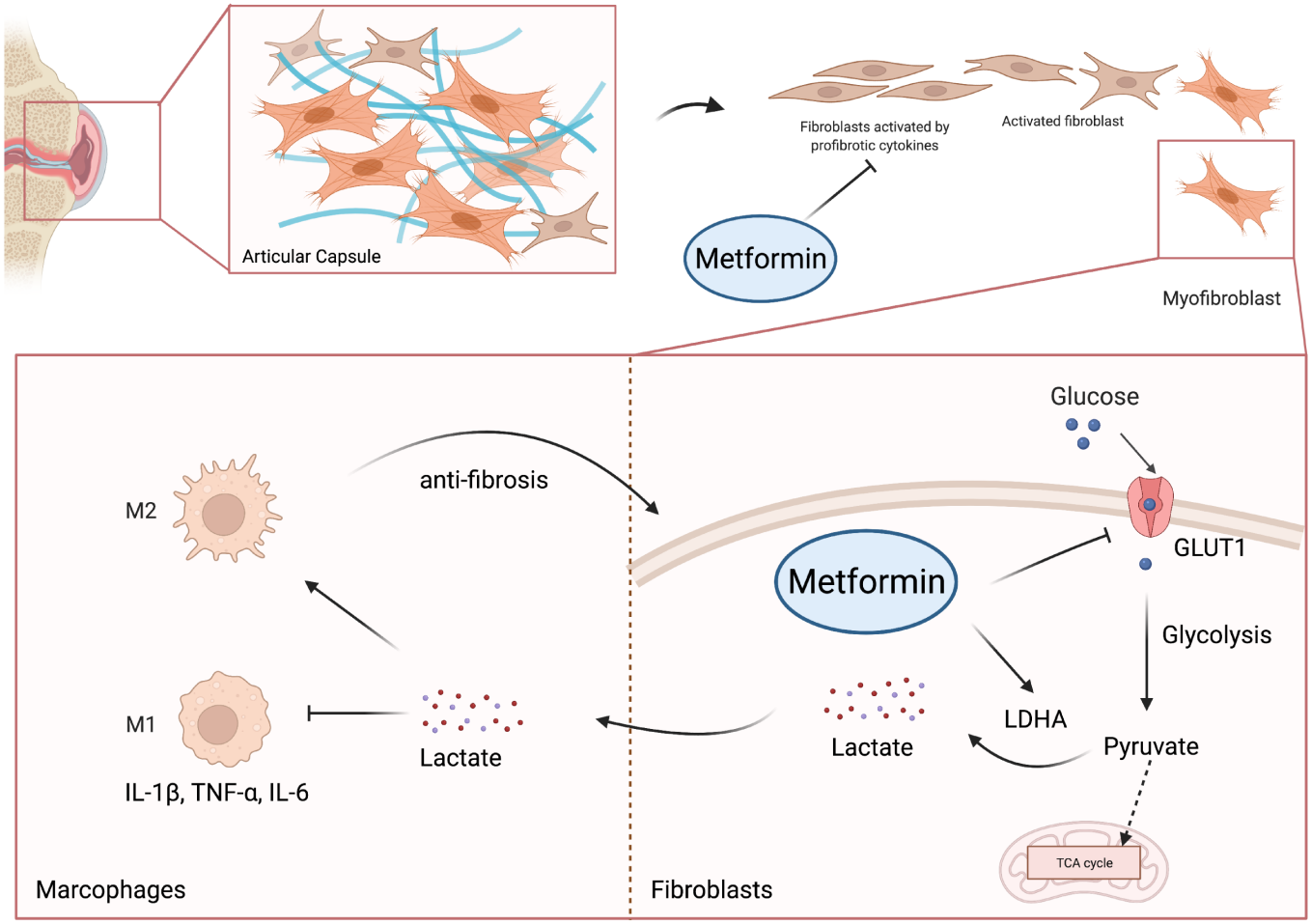
Articular Capsule
Fibroblasts activated by profibrotic cytokines
Activated fibroblast
Metformin
Myofibroblast
anti-fibrosis
M2
M1
IL-1β, TNF-α, IL-6
Lactate
Marcophages
Glucose
GLUT1
Metformin
Glycolysis
LDHA
Lactate
Pyruvate
TCA cycle
Fibroblasts

A

B

C

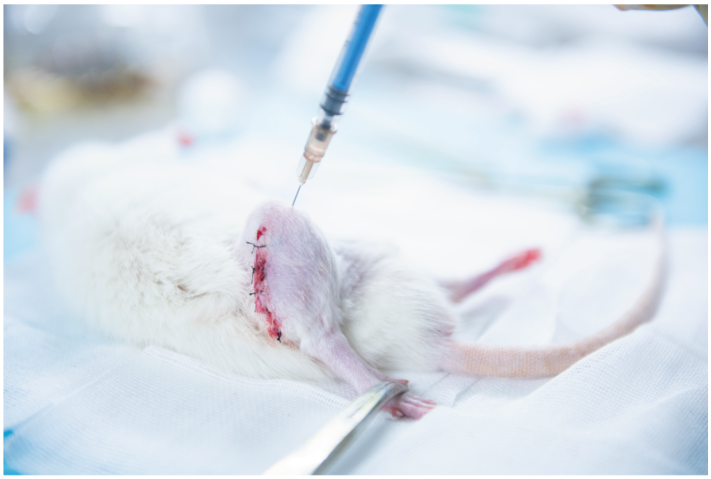

Suppl-2

Genes	Primer sequence (5'-forward primers-3')	Primer sequence (5'-reverse primers-3')
h-GLUT1	TGGCATCAACGCTGTCTTCT	AACAGCGACACGACAGTGAA
h-TGF-β1	TGGAGAGAGGACTGCGGAT	CTGGTCCCCTGTGCCTTGAT
h-α-SMA	AGGGAAGGTCCTAACAGCCC	AGGATTCCCGTCTTAGTCCC
h-FN1	ACAAGCATGTCTCTCTGCCAA	GCAATGTGCAGCCCTCATTT
h-HK2	GAGGAACCAATTTCCGTGCTGCT	CCTTTGATCCCCATGTAGTCCAAGA
h-PKM	TCGCATGCAGCACCTGATT	CCTCGAATAGCTGCAAGTGGTA
h-PFKP	AATTATGGATCCATGACCCATGAAGAGCACC	AATTATTCTAGATTAGACGGCCGCTTCCCC
h-PFKFB3	CAGTTGTGGCCTCCAATATC	GGCTTCATAGCAACTGATCC
h-LDHA	CCGACGTGCATTCCCGAT	GAGCAAGTTCATCTGCCAAGT
h-β-ACTIN	TGGAACGGTGAAGGTGACAG	AACAACGCATCTCATATTTGGAA
Genes	Primer sequence (5'-forward primers-3')	Primer sequence (5'-reverse primers-3')
m-GLUT1	CTGTGAGTTCCTGAGACCCTG	CCCAGGCAAGGAAGTAGTTC
m-α-SMA	GTACCACCATGTACCCAGGC	GCTGGAAGGTAGACAGCGAA
m-FN1	TCAGAAGAGTGAGCCCCTGA	CAGGGTTGGTGATGAAGGGG
m-HK2	GCTACCCGGAGTTGTTCTGC	CTAAGTCTCACTCCTGCCGAC
m-PKM	TCGAGGAACTCCGCCGCCTG	CCACGGCACCCACGGCGGCA
m-PFKP	TGTGGTCCGAGTTGGTATCTT	GCACTTCCAATCACTGTGCC
m-LDHA	GCGGAGCTTCCATTTAAGGC	GGGTTGCCATCTTGGACTTTG
m-TNF-α	TCAGCCTCTTCTCATTCCTGCT	CCATTTGGGAACTTCTCATCCCT
m-IL-1β	CGTTCCCATTAGACAACTGCACT	TTTCAGCTCATATGGGTCCGACA
m-IL-6	ACAAGTCGGAGGCTTAATTACACA	ATCCAGTTTGGTAGCATCCATCA
m-iNOS	GCCCAGCCAGCCCAAC	GCAGCTTGTCCAGGGATTCT
m-CD163	TGCTGTCACTAACGCTCCTG	TCATTCATGCTCCAGCCGTT
m-Arg-1	AGCTTCGTAAAATCGCTGGGA	AGGACAATGTGTACGCGACT
m-β-ACTIN	AGCCTCGCCTTTGCCGA	CTGGTGCCTGGGGCG
Gene	**siRNA sequences (5`-forward-3`)**	siRNA sequences (5`-reverse-3`)
siLDHA-1	CCUUGUUGACGUCAUGGAATT	UUCCAUGACGUCAACAAGGTT
siLDHA-2	CGUGAACAUCUUCAAGUUCAU	AUGAACUUGAAGAUGUUCACG
siLDHA-3	CGUCUCCCUGAAGUCUCUUAA	UUAAGAGACUUCAGGGAGACG
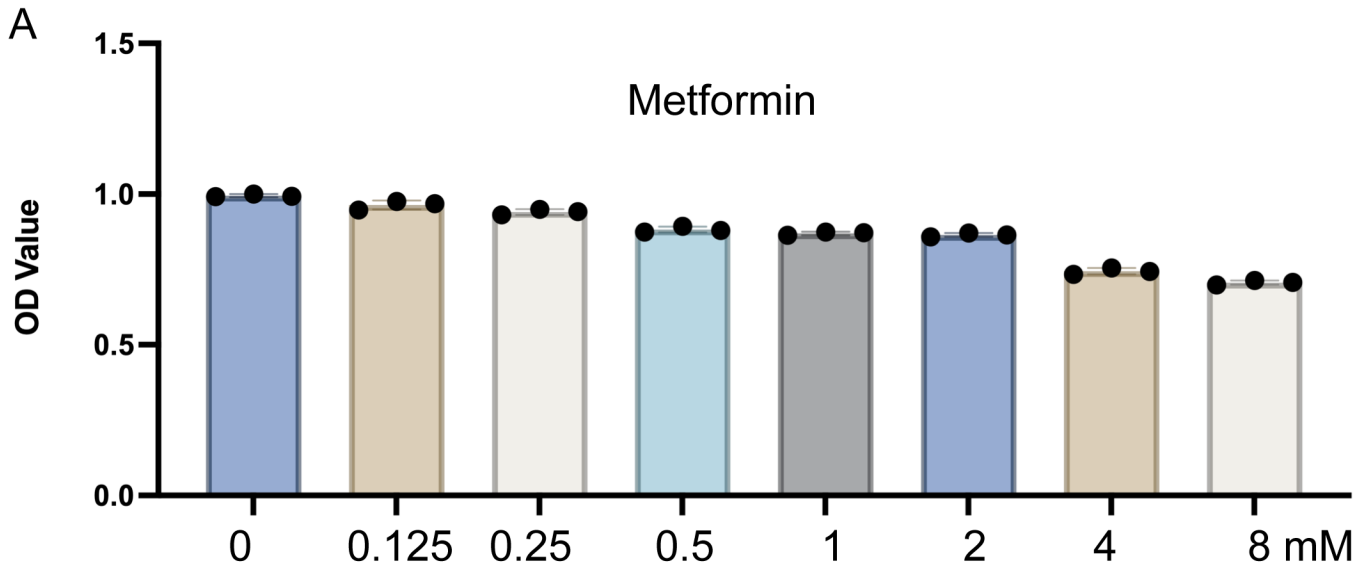
Suppl-3